

Block-Coordinate Descent on the Riemannian Staircase for Certifiably Correct Distributed Rotation and Pose Synchronization

Yulun Tian, Kasra Khosoussi, and Jonathan P. How*

November 12, 2019

Abstract

This paper presents the first *certifiably correct* solver for distributed pose-graph optimization (PGO), the backbone of modern collaborative simultaneous localization and mapping (CSLAM) and camera network localization (CNL) systems. By pursuing a sparse semidefinite relaxation, our approach provides formal performance guarantees that match state-of-the-art centralized techniques. In particular, under low noise, the proposed distributed solver is guaranteed to find *globally optimal* solutions despite the non-convexity of PGO. To solve the resulting large-scale semidefinite programs, we adopt the state-of-the-art Riemannian Staircase framework and develop Riemannian block-coordinate descent (RBCD) as the core distributed local search algorithm. RBCD is well-suited to distributed synchronization problems (such as rotation and pose synchronization) as it only requires local communication, provides privacy protection, and is easily parallelizable. Furthermore, we prove that RBCD converges to first-order critical points for general Riemannian optimization problems over product manifolds, and establish a *global* sublinear convergence rate. Extensive evaluations on real and synthetic PGO datasets demonstrate state-of-the-art performance of the proposed distributed solver.

arXiv:1911.03721v1 [math.OC] 9 Nov 2019

*The authors are with the Laboratory for Information and Decision Systems (LIDS), Massachusetts Institute of Technology, Cambridge, MA. {yulun, kasra, jhow}@mit.edu

Contents

1	Introduction	4
2	Related Work	6
2.1	Centralized Solvers	6
2.2	Decentralized Solvers	7
2.3	Block-Coordinate Descent	7
3	Certiably Correct Pose-Graph Optimization	8
3.1	Pose-Graph Optimization (PGO)	8
3.1.1	Rotation Synchronization	8
3.1.2	Pose Synchronization	9
3.1.3	Distributed PGO	9
3.2	SDP Relaxation for PGO	10
3.3	The Riemannian Staircase Algorithm	11
4	Riemannian Block-Coordinate Descent	12
4.1	Block Selection Rules	14
4.2	Block update with Riemannian Trust-Region (RTR)	14
4.3	Optimal Update for Single Rotation	15
4.4	Optimal Update for Single Pose	16
4.5	Parallel Execution	16
5	Convergence Analysis for RBCD	18
6	Distributed Initialization, Verification, and Rounding	21
6.1	Distributed Initialization	21
6.2	Distributed Verification	21
6.3	Distributed Rounding	22
7	Experiments	22
7.1	CSLAM Experiments	23
7.1.1	Convergence vs. RGD	23
7.1.2	Varying Noise Level	24
7.1.3	Varying Number of Robots	26
7.1.4	Varying Inter-robot Connectivity	26
7.1.5	Performance on Benchmark Datasets	27
7.2	CNL Experiments	28
7.2.1	Convergence vs. RGD and RBR	29
7.2.2	Varying Rank Relaxation	29
8	Conclusion	30
	Appendices	36
A	Proof of Theorem 1	36
B	Proof of Theorem 2	38
C	Proof of Corollary 1	40

D Proof of Lemma 1	40
E Proof of Lemma 2	42
F Proof of Theorem 3	44

1 Introduction

Collaborative simultaneous localization and mapping (CSLAM) is a fundamental capability for multi-robot systems navigating in unknown GPS-denied environments. CSLAM allows robots to leverage the observations acquired by their peers to improve their own spatial awareness. Additionally, it provides a consistent spatial understanding across the team, which is a key requisite for more complex modes of collaboration in multi-robot missions. In this work, we focus on the back-end stage of modern CSLAM and camera network localization (CNL) systems, in which robots *collaboratively* solve a pose-graph optimization (PGO) problem to estimate their trajectories based on noisy relative measurements.

Centralized schemes for collaborative PGO (e.g., [1]) are suitable only for limited scenarios as they require a number of restrictive assumptions: a central node that is capable of solving the entire team’s PGO problem; a sufficiently reliable communication channel that connects the central node to the team; and enough resources (mainly, energy and bandwidth) for regularly relaying the team’s (raw or preprocessed) observations to the central node. Additionally, these schemes do not protect the privacy of their participants (since the central node would have access to the entire team’s observations and trajectories) and are less robust due to having a single point of failure. These critical issues demonstrate the need for decentralized and distributed PGO solvers for CSLAM and CNL.

State-of-the-art decentralized and distributed back-ends [2–4] have fallen behind recent breakthroughs that have led to *certifiably correct* centralized PGO solvers based on semidefinite relaxations [5–9]. Specifically, these distributed solvers inherit the conventional nonlinear least squares approach to solve PGO which is susceptible to suboptimal solutions and arbitrarily bad local minima. In contrast, state-of-the-art centralized approaches attain *global optimality* by relaxing PGO into a tractable semidefinite program (SDP). Among these works, Rosen et al. [5] further show that under prevalent low-to-moderate noise regimes, one can recover the *unique global minimizer* (up to global gauge symmetry) to PGO via SDP relaxation. Such *a priori* performance guarantees thus provide strong theoretical justifications on why SDP-based approaches are favorable.

The main goal of this paper is to fill the aforementioned technical gap by designing *certifiably correct* decentralized and distributed PGO solvers. To this end, we pursue an alternative SDP relaxation [6] for pose synchronization that avoids the elimination of translation variables and thus preserves the essential sparsity structure for distributed optimization (see Remark 1). As our first contribution, we provide formal performance guarantees for this SDP relaxation by showing that it shares the same set of core theoretical properties with the original SDP relaxation of Rosen et al. [5], in terms of the *existence of low-rank solutions* (Theorem 1) and *exactness guarantees under low noise* (Theorem 2).

Our second contribution is the design and analysis of a *distributed* algorithm for solving the SDP relaxations of PGO. In practice, the typical sizes of these SDPs make standard interior-point methods infeasible. To attain comparable speed with conventional SLAM solvers, state-of-the-art centralized approaches employ a technique known as the Riemannian Staircase [10] in which one solves a hierarchy of rank-restricted SDPs using the celebrated Burer-Monteiro factorization [11]. At each level of the hierarchy, a local search is performed to find critical points of the rank-restricted problem. In the centralized setting, the second-order Riemannian trust-region (RTR) algorithm [12, 13] has emerged as the default method to carry out the local search. Nevertheless, RTR (or similar second-order methods) requires a second-order model of the cost function and delicate bookkeeping of parameters (e.g., the trust-region radius), both of which make the algorithm unsuitable for distributed computation.

To address this challenge, we propose Riemannian block-coordinate descent (RBCD) as the core distributed procedure to solve the rank-restricted SDP relaxations of PGO inside the Riemannian Staircase framework. RBCD is a general algorithm for optimization over direct product of matrix submanifolds. Under mild conditions, we show that the algorithm converges to first-order critical points with *global* sublinear convergence rate. Furthermore, RBCD *exploits the special structures* in typical CSLAM and CNL problems. Specifically, by leveraging the sparsity structure and independence relations in the pose graph, RBCD retains the critical features of state-of-the-art distributed solvers [2]:

- Simple iterations: agents locally perform simple (and *closed-form* in the case of CNL) updates during

optimization.

- Local communication: agents only need to communicate with their neighbors (i.e., those connected by loop closures) in the pose graph.
- Privacy protection: during optimization, agents do not reveal information about their “private” states and observations.
- Parallel execution: at each iteration, multiple agents update in parallel without compromising the correctness of their solutions.

The rest of this paper is organized as follows. In Section 2, we review state-of-the-art centralized and distributed solvers for PGO, as well as recent advances in block-coordinate optimization methods. In Section 3, we review the problem formulation of PGO, its SDP relaxation, as well as the Riemannian Staircase framework. As our first contribution, we also present formal guarantees for the alternative SDP relaxation of pose synchronization used in this work. In Section 4, we present the RBCD algorithm. In Section 5, we prove convergence of RBCD and provide global convergence rate analysis. We discuss several details related to the distributed implementation of Riemannian Staircase in Section 6. We conclude with extensive experimental evaluations in Section 7.

Notations and Preliminaries

General Notations

Lowercase and uppercase letters are reserved for vectors and matrices, respectively. We use $[n]$ to denote the set of natural numbers up to and including n . Unless specified otherwise, letters i, j, k refer to indices of single poses or rotations, and α, β, γ refer to indices of robots.

Linear Algebra

\mathbb{S}^d and $\mathbb{S}_{\geq 0}^d$ denote the set of $d \times d$ symmetric and symmetric positive semidefinite matrices, respectively. $I_d \in \mathbb{R}^{d \times d}$ is the identity matrix, and $0_d, 1_d \in \mathbb{R}^d$ represent the vectors of all zeros and all ones, respectively. For a matrix M , we use $M_{(i,j)}$ to index its (i, j) -th entry. Given a $(d \times d)$ -block-structured matrix $M \in \mathbb{R}^{dn \times dn}$, $M_{[i,j]} \in \mathbb{R}^{d \times d}$ refers to its (i, j) -th block. Following [5], we define $\text{BlockDiag}(M)$ as the linear operator that extracts the diagonal blocks of M and zeros out all remaining blocks, and $\text{SymBlockDiag}_d(M)$ as its symmetric version; see [5, Equations (4)-(5)]. Finally, $\text{Proj}_{\mathcal{S}}$ denotes the projection operator onto a given set \mathcal{S} .

Differential Geometry and Lie Groups

The orthogonal group is defined as,

$$\text{O}(d) \triangleq \{R \in \mathbb{R}^{d \times d} \mid R^\top R = I_d\}. \quad (1)$$

The special orthogonal group is defined as,

$$\text{SO}(d) \triangleq \{R \in \mathbb{R}^{d \times d} \mid R^\top R = I_d, \det(R) = 1\}. \quad (2)$$

The special Euclidean group is defined as,

$$\text{SE}(d) \triangleq \left\{ \begin{bmatrix} R & t \\ 0_d^\top & 1 \end{bmatrix} \mid R \in \text{SO}(d), t \in \mathbb{R}^d \right\}. \quad (3)$$

The Stiefel manifold is defined as,

$$\text{St}(d, r) \triangleq \{Y \in \mathbb{R}^{r \times d}, Y^\top Y = I_d\}. \quad (4)$$

In general, we use \mathcal{M} to denote a smooth matrix submanifold. For two manifolds $\mathcal{M}_1, \mathcal{M}_2$, $\mathcal{M}_1 \times \mathcal{M}_2$ denotes their product manifold. \mathcal{M}^n denotes the n -th power manifold of \mathcal{M} . Following [5], we represent the product manifold and power manifold in matrix form as,

$$\mathcal{M}_1 \times \mathcal{M}_2 \triangleq \left\{ \begin{bmatrix} x_1 & x_2 \end{bmatrix} \mid x_1 \in \mathcal{M}_1, x_2 \in \mathcal{M}_2 \right\}. \quad (5)$$

$$\mathcal{M}^n \triangleq \left\{ \begin{bmatrix} x_1 & \dots & x_n \end{bmatrix} \mid x_i \in \mathcal{M}, \forall i \in [n] \right\}. \quad (6)$$

On the manifold, $T_x\mathcal{M}$ (or T_x for brevity) denotes the tangent space at $x \in \mathcal{M}$. The tangent space is endowed with the standard Riemannian metric induced from the ambient (Euclidean) space, i.e., $\langle \eta_1, \eta_2 \rangle \triangleq \text{tr}(\eta_1^\top \eta_2)$, and the induced norm is $\|\eta\| \triangleq \sqrt{\langle \eta, \eta \rangle}$. Retr denotes a retraction operator, with $\text{Retr}_x : T_x\mathcal{M} \rightarrow \mathcal{M}$ being its restriction to $T_x\mathcal{M}$. For a function $f : \mathcal{M} \rightarrow \mathbb{R}$, we use $\nabla_x f$ and $\text{grad}_x f$ to denote the Euclidean and Riemannian gradients of f at $x \in \mathcal{M}$. We call $x^* \in \mathcal{M}$ a *first-order* critical point if the corresponding Riemannian gradient is zero. Readers are referred to [13] for a comprehensive review of relevant differential geometry concepts.

2 Related Work

2.1 Centralized Solvers

Rosen et al. [5] developed SE-Sync, a state-of-the-art certifiably correct solver for PGO. SE-Sync solves a SDP relaxation of PGO after analytically eliminating translation variables [14]. It is shown that under low noise, the SDP relaxation is guaranteed to be exact and hence can be used to extract a globally optimal solution to the original PGO problem. In addition to the theoretical low-noise guarantee, in [5] it is also empirically demonstrated that global optimality holds under typical noise levels encountered in robotic applications.

Despite the need to solve a large-scale SDP, SE-Sync often outperforms conventional sparse nonlinear least squares solvers in terms of runtime. This is mainly attributed to the Riemannian Staircase algorithm [10] which leverages the so-called Burer-Monteiro factorization [11] to search for low-rank solutions of the SDP. The Riemannian Staircase requires a numerical optimization algorithm to search for (ideally second-order) critical points of a non-convex optimization problem over the product of Stiefel manifolds. By default, SE-Sync uses the second-order Riemannian trust-region (RTR) method [12, 13]. RTR is a popular method due to a number of remarkable features including provable global convergence to second-order critical points and superlinear local convergence rate. In order to avoid inverting the Riemannian Hessian at each iteration, “inverse-free” techniques such as truncated conjugate gradient (tCG) are frequently used inside RTR to solve each trust-region subproblem. Nevertheless, both RTR and tCG require delicate bookkeeping (e.g., for updating the trust-region radius in RTR and descent direction in tCG) which makes the overall algorithm inherently centralized.

A similar centralized solver is proposed by Briaies and Gonzalez-Jimenez [6]. The main difference between SE-Sync and Cartan-Sync [6] is that the latter directly performs SDP relaxation over PGO without first analytically eliminating the translations. As a result, the rank-restricted problems solved inside the Riemannian Staircase are defined over the direct product of Stiefel manifolds and the Euclidean space. Because of the non-compactness of this search space, the low-noise global optimality guarantees of [5] have not been extended to this case.

Similar SDP relaxations [7, 9, 15] have also been proposed for the closely related problem of angular synchronization and rotation synchronization (also known as rotation averaging [16] or synchronization over the special orthogonal group). This fundamental problem arises in a number of domains such as CNL [17–19] and cryo-EM in structural biology. In particular, rotation synchronization is a crucial intermediate step in bundle adjustment for structure from motion [16]. In this work, we consider rotation synchronization as a special class of PGO, and show that the proposed approach directly covers this problem.

This work follows a similar path as [5, 6] and considers solving the SDP relaxations of PGO *distributedly*. Due to the need to preserve sparsity for distributed optimization (see Remark 1), we choose to pursue the alternative (sparse albeit non-compact) SDP relaxation used in [6]. As one of our main contributions, we

address the open problem concerning the theoretical properties of this SDP relaxation. In Section 3, we show that despite non-compactness, the alternative SDP relaxation enjoys the same performance guarantees as the original SDP relaxation employed by SE-Sync [5]. This result serves as a strong theoretical foundation that motivates us to design efficient distributed solvers in Section 4.

2.2 Decentralized Solvers

The work by Choudhary et al. [2] is currently the state of the art in distributed PGO solvers and has been recently used by modern decentralized CSLAM systems [20, 21]. In [2] the authors propose a two-stage approach for finding approximate solutions to PGO. The first stage estimates the rotation variables by forming and solving a linear least squares problem after relaxing the non-convex rotation constraints. The resulting solution is then projected back to the rotation group. The rotation estimates are then used in the second stage to initialize a single Gauss-Newton iteration on the full pose synchronization problem. In both stages, classical distributed techniques such as Jacobi over-relaxation (JOR) and successive over-relaxation (SOR) [22] are used to solve the normal equations of the linear least squares problems. The experimental evaluations presented in [2] demonstrate that this approach significantly outperforms prior techniques [3, 4]. Nonetheless, [2] is still performing incomplete local search on a non-convex problem and thus does not offer any global performance guarantees.

In another line of work, Tron et al. [17–19] propose a multi-stage distributed Riemannian consensus protocol for CNL based on distributed execution of Riemannian gradient descent over \mathcal{M}^n where $\mathcal{M} = \text{SO}(3) \times \mathbb{R}^3$ and n is the number of cameras (agents). CNL can be seen as a special instance of collaborative PGO where each agent owns a *single* pose rather than an entire trajectory. In these works, the authors establish convergence to critical points and, under *perfect* (i.e., noiseless) measurements, convergence to globally optimal solutions. We present a specialized form of our distributed PGO algorithm for CNL in Sections 4.3 and 4.4.

2.3 Block-Coordinate Descent

Block-coordinate descent (BCD) methods (also known as Gauss-Seidel-type methods) are classical techniques [22] that have recently regained popularity in large-scale machine learning and numerical optimization [23–25]. These inherently simple methods have cheap iterations and are often easily distributable and parallelizable [22].

In SLAM, BCD-type techniques have been applied in the past [26, 27]. In computer vision, variants of the Weiszfeld algorithm have also been used for robust rotation averaging [16, 28]. The abovementioned techniques, however, do not guarantee global optimality in rotation or pose synchronization problems. More recently, Eriksson et al. [29, 7] propose a BCD-type algorithm for solving the SDP relaxation of rotation synchronization. Their row-by-row (RBR) solver extends the approach proposed in [30] from SDPs with diagonal constraints to block-diagonal constraints. In small problems with up to $n = 300$ rotations, this approach is shown to be comparable or better than the Riemannian Staircase approach [10] in terms of runtime [7]. This approach, however, needs to store and manipulate a *dense* $dn \times dn$ matrix which is not sustainable in SLAM where in typical moderate-size problems, n is one to two orders of magnitude larger than the problems considered in [7]. We provide a runtime comparison between RBR [7] and our algorithm in Section 7.2. Finally, although in principle this algorithm can be executed distributedly, the resulting scheme would not preserve the privacy of the participants.

This work is originally inspired by recent block-coordinate minimization algorithms proposed in [31, 32] for solving SDPs with diagonal constraints via the Burer-Monteiro approach. Our recent technical report [33] extends these algorithms and the global convergence rate analysis provided by Erdogdu et al. [32] from the unit sphere (diagonal constraints) to the Stiefel manifold (block-diagonal constraints). In this work, we further extend our initial results [33] by providing a unified Riemannian BCD algorithm and its global convergence rate analysis, as well as proposing specialized scheme for collaborative pose/rotation synchronization.

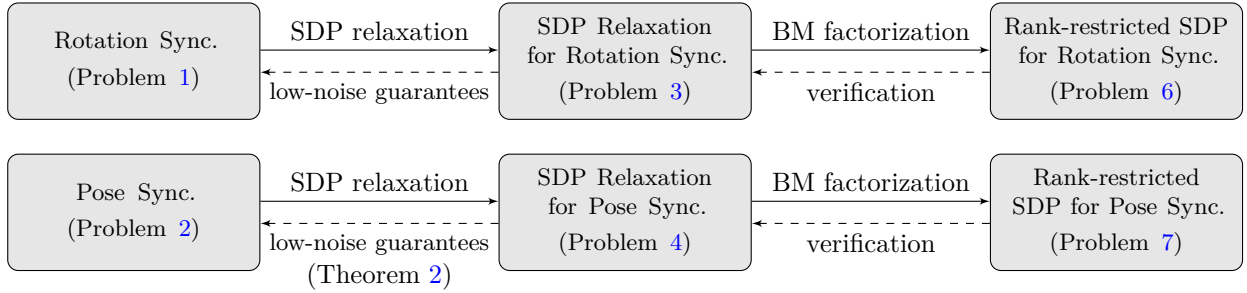


Figure 1: Relations between problems considered in this work. From the original PGO problem (rotation or pose synchronization), applying semidefinite relaxation yields the corresponding SDPs. Applying Burer-Monteiro (BM) factorization [11] on the SDPs then yields the rank-restricted SDPs which can be solved with Riemannian local search algorithms. Solutions to the SDPs can be recovered from solutions to their rank-restricted surrogates via post-hoc verification (Section 6.2). Finally, under sufficiently low noise, SDP relaxations are guaranteed to find *global* minimizers to PGO (e.g., see Theorem 2).

3 Certifiably Correct Pose-Graph Optimization

In this section, we formally introduce the pose-graph optimization (PGO) problem. We also review state-of-the-art *certifiably correct* PGO solvers based on SDP relaxations, together with how these SDPs are solved in practice using the Riemannian Staircase framework. Figure 1 summarizes the problems we introduce in this section and how they relate to each other. As our first technical contribution, we establish formal guarantees for the alternative SDP relaxation of PGO [6] used in this work; see Theorem 1 and Theorem 2.

3.1 Pose-Graph Optimization (PGO)

In PGO, we need to estimate n unknown rotations or poses from a set of noisy relative measurements. In graph terms, PGO can be modeled with a directed graph (pose graph) $\mathcal{G} = (\mathcal{V}, \mathcal{E})$, where $\mathcal{V} = [n]$ and $\mathcal{E} \subseteq \mathcal{V} \times \mathcal{V}$ correspond to the sets of unknown poses and relative measurements, respectively. In the rest of this paper, we make the standard assumption that \mathcal{G} is weakly connected.

3.1.1 Rotation Synchronization

In some applications, the unknown variables consist only of rotations rather than of full poses. Examples include CNL [18, 19], structure from motion pipelines [7], and initialization techniques for SLAM [34]. In these cases, the estimation problem is more frequently referred to as *rotation synchronization* or *rotation averaging*. Let $R_1, R_2, \dots, R_n \in \text{SO}(d)$ denote the set of rotation variables. Following [5], we assume that for each edge $(i, j) \in \mathcal{E}$, the corresponding relative rotation measurement is generated from a Langevin distribution,

$$\tilde{R}_{ij} = \underline{R}_{ij} R_{ij}^\epsilon, R_{ij}^\epsilon \sim \text{Langevin}(I_d, \kappa_{ij}), \quad (7)$$

where $\underline{R}_{ij} \triangleq \underline{R}_i^\top \underline{R}_j$ denotes the ground truth relative rotation.

Under noise model (7), it can be shown that the maximum likelihood estimate (MLE) corresponds to the minimizer of the following non-convex optimization problem,

Problem 1 (Rotation Synchronization).

$$\underset{R_1, \dots, R_n}{\text{minimize}} \quad \sum_{(i,j) \in \mathcal{E}} \kappa_{ij} \|R_j - R_i \tilde{R}_{ij}\|_F^2, \quad (8a)$$

$$\text{subject to} \quad R_i \in \text{SO}(d), \forall i \in [n]. \quad (8b)$$

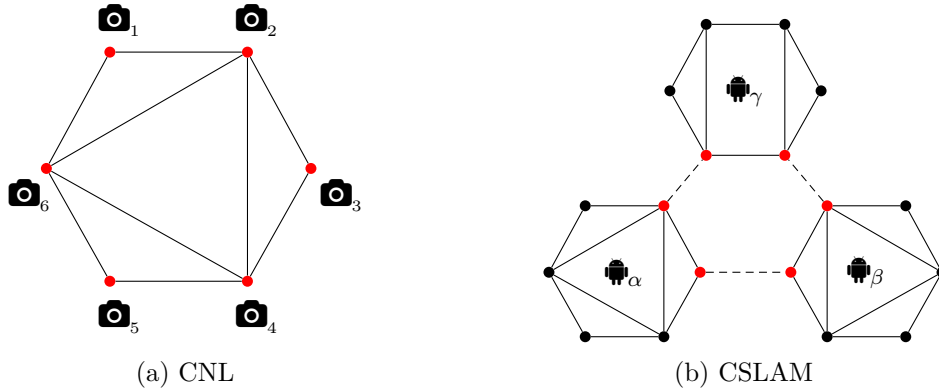


Figure 2: Distributed PGO scenarios considered in this work. (a) In CNL, a group of cameras need to localize each other in a common reference frame. Each vertex in the pose graph denotes the pose of a single camera. Cameras that share overlapping fields of view are connected by relative measurements. (b) In CSLAM, multiple robots need to jointly estimate their trajectories in the same frame. Each robot has multiple pose variables that are connected by odometric measurements and loop closures. We refer to poses that have inter-robot loop closures (dashed edges) as public (marked in red), and all other poses as private (marked in black).

3.1.2 Pose Synchronization

Next, we consider estimation of full pose variables which is the default setup in pose-graph SLAM. Analogous to Problem 1, this problem is also known as *pose synchronization* or *motion averaging*. Each variable is now an element from the special Euclidean group, represented (with a slight abuse of notation) as $T_i = \begin{bmatrix} R_i & t_i \end{bmatrix} \in \text{SE}(d)$, where $t_i \in \mathbb{R}^d$ represents the translation component of pose i . In addition to the relative rotation measurements (7), we also obtain relative translation measurements corrupted by additive Gaussian noise,

$$\tilde{t}_{ij} = \underline{t}_{ij} + t_{ij}^\epsilon, t_{ij}^\epsilon \sim \mathcal{N}(0, \tau_{ij}^{-1} I_d), \quad (9)$$

where $\underline{t}_{ij} \triangleq \underline{R}_i^\top (\underline{t}_j - \underline{t}_i)$ denotes the ground truth relative translation. The MLE of pose synchronization corresponds to the minimizer of the following problem,

Problem 2 (Pose Synchronization).

$$\underset{\{R_i\}, \{t_i\}}{\text{minimize}} \quad \sum_{(i,j) \in \mathcal{E}} \kappa_{ij} \|R_j - R_i \tilde{R}_{ij}\|_F^2 + \tau_{ij} \|t_j - t_i - R_i \tilde{t}_{ij}\|_2^2, \quad (10a)$$

$$\text{subject to} \quad R_i \in \text{SO}(d), t_i \in \mathbb{R}^d, \forall i \in [n]. \quad (10b)$$

3.1.3 Distributed PGO

In this work, we focus on solving Problem 1 and 2 in the *distributed* setting. More specifically, we consider two important real-world applications: CNL and CSLAM. In CNL, a network of cameras need to localize each other with respect to a common reference. In this case, each vertex in the pose graph represents the rotation or pose of a single camera. Relative measurements are extracted between camera pairs with overlapping fields of view using standard two-view geometry techniques and subject to scale ambiguity in the case of monocular cameras. See Figure 2a for a simple illustration.

In CSLAM, multiple robots need to jointly estimate their trajectories in a common reference frame. In the pose graph, each vertex represents the pose of a robot at a certain time step. Odometric measurements and *intra-robot* loop closures connect poses within a single robot's trajectory. When two robots visit the same part of the environment, they establish *inter-robot* loop closures that link their respective poses at that time step.

See Figure 2b for a simple example. In this case, we can further divide vertices into two classes based on they have inter-robot loop closures.

Definition 1 (Public and private poses in CSLAM). In CSLAM, all poses that share inter-robot loop closures with poses of other robots are called *public* poses. All other poses are *private* poses.

In the literature, public poses are also known as the *separators* [4]. In Figure 2b, public poses are marked in red and private poses are marked in black. We note that with this definition, all poses in CNL would be characterized as public since each agent (camera) only has a single pose.

3.2 SDP Relaxation for PGO

Traditionally, Problem 1 and 2 are solved with local search algorithms such as Gauss-Newton. However, depending on the noise level and the quality of initialization, local search algorithms are susceptible to local minima [35]. To address this critical issue, recent works aim to develop certifiably correct *global* PGO solvers. In particular, techniques based on SDP relaxation demonstrate state-of-the-art performance and furthermore provide strong theoretical guarantees under low noise regimes [5, 7, 9]. In this section, we present SDP relaxations for Problems 1 and 2.

We begin with rotation synchronization (Problem 1). Let $R = [R_1 \ R_2 \ \dots \ R_n] \in \text{SO}(d)^n$ denote the stacked rotation variables. It can be shown that the cost function (8a) in Problem 1 can be equivalently written as $\text{tr}(Q_R R^\top R)$, where $Q_R \in \mathbb{S}_{\geq 0}^{dn}$ is the so-called *connection Laplacian* matrix [5]. Consider the “lifted” variable $Z_R = R^\top R \in \mathbb{S}_{\geq 0}^{dn}$. Treating Z_R as a $(d \times d)$ -block-structured matrix, we can rewrite the constraints (8b) in Problem 1 as $Z_R \succeq 0$, $Z_{R[i,i]} = I_d$ for $i \in [n]$, $\text{rank}(Z_R) = d$, and $\det(Z_{R[i,j]}) = 1$ for all $i, j \in [n]$. Dropping the last two non-convex constraints yields the following SDP relaxation for Problem 1.

Problem 3 (SDP Relaxation for Rotation Synchronization).

$$\underset{Z_R \in \mathbb{S}_{\geq 0}^{dn}}{\text{minimize}} \quad \text{tr}(Q_R Z_R) \tag{11a}$$

$$\text{subject to} \quad Z_{R[i,i]} = I_d, \forall i \in [n]. \tag{11b}$$

Following similar steps, one can derive the SDP relaxation for the pose synchronization problem (see [6] for the detailed derivations). Denote the connection Laplacian of Problem 2 as $Q_T \in \mathbb{S}_{\geq 0}^{n+dn}$, and treat the SDP variable $Z_T \in \mathbb{S}_{\geq 0}^{n+dn}$ as a $[(d+1) \times (d+1)]$ -block-structured matrix. Then, the SDP relaxation is given by,

Problem 4 (SDP Relaxation for Pose Synchronization).

$$\underset{Z_T \in \mathbb{S}_{\geq 0}^{n+dn}}{\text{minimize}} \quad \text{tr}(Q_T Z_T) \tag{12a}$$

$$\text{subject to} \quad Z_{T[i,i](1:d,1:d)} = I_d, \forall i \in [n]. \tag{12b}$$

In the original SE-Sync algorithm [5], Rosen et al. employ a different SDP relaxation for Problem 2 by first using the separable structure of PGO [14] to analytically eliminate the translation variables, and subsequently performing convex relaxation over the reduced rotation-only problem. The resulting SDP has the form,

Problem 5 (Rotation-only SDP Relaxation for Pose Synchronization [5]).

$$\underset{Z_R \in \mathbb{S}_{\geq 0}^{dn}}{\text{minimize}} \quad \text{tr}(\tilde{Q}_T Z_R) \tag{13a}$$

$$\text{subject to} \quad Z_{R[i,i]} = I_d, \forall i \in [n]. \tag{13b}$$

In (13a), \tilde{Q}_T is a *dense* cost matrix, and is essentially the generalized Schur complement of the sparse connection Laplacian Q_T (see Appendix A). As the first technical contribution in this section, we establish the following theorem which characterizes key relations between Problem 4 and Problem 5.

Theorem 1 (Relations between Problem 4 and Problem 5). Problem 4 admits a minimizer Z_T^* with $\text{rank}(Z_T^*) = r$ if and only if Problem 5 admits a minimizer Z_R^* with the same rank. Furthermore, $\text{tr}(Q_T Z_T^*) = \text{tr}(\tilde{Q}_T Z_R^*)$ for all minimizers of Problem 4 and Problem 5.

Theorem 1 suggests that, for pose synchronization, the elimination of translation variables does not affect the optimal value or the rank of solutions in the SDP relaxation. This result has a far-reaching impact, as it further allows us to establish equivalent *low-noise guarantees* for the two SDP relaxations. Specifically, Rosen et al. [5] show that under low noise, the rotation-only SDP (Problem 5) is *exact*, i.e., from its solution one can recover a *global* minimizer to the original non-convex pose synchronization problem (see [5, Proposition 2]). Using Theorem 1 and [5, Proposition 2], we show that the same a priori guarantee can be established for our SDP relaxation (Problem 4), which is first used in Cartan-Sync [6] albeit without exactness guarantees. We give an informal statement below, and provide the formal theorem and its proof in Appendix B.

Theorem 2 (Exact recovery via Problem 4 (Informal)). Under sufficiently low measurement noise, every minimizer Z_T^* to Problem 4 has its first $d \times (n + dn)$ block row given by $Z_{T(1:d,:)}^* = [R_1^* \ t_1^* \ \dots \ R_n^* \ t_n^*]$, where $\{R_i^*, t_i^*\}$ is an optimal solution to Problem 2.

Theorem 2 provides a strong theoretical justification on why we solve Problem 4 — under low noise (which we characterize in Appendix B), one can directly read off a global minimizer to Problem 2 from the first block row of any Z_T^* . We note that the low noise requirement is usually satisfied on real-world datasets (see Section 7). A similar result can be established for rotation synchronization (e.g., using a subset of the machinery in [5]; see also [7] for a similar result).

Remark 1. Here we explain why we refrain from pursuing the original SDP relaxation (Problem 5) used by SE-Sync [5] in this work. Problem 5 enjoys several benefits including having a compact search space and better numerical conditioning. However, the cost matrix \tilde{Q}_T in Problem 5 is *dense* due to the Schur complement operation (see Appendix A). In graph terms, eliminating the translation variables makes the underlying dependency graph *fully connected*. This is a major drawback in the distributed setting since robots’ public and private poses become fully dependent on other robots’ trajectories which increases the communication costs substantially. As we shall see in the following sections, our proposed algorithms rely on and exploit the sparse (inter/intra-robot) graphical structure of the problem to achieve computational and communication efficiency, and to preserve the privacy of participating robots. For this reason, in this work we adopt the alternative approach of [6] which directly relaxes the original problem and thus preserves the essential sparsity structure (e.g., as in Figure 2a and 2b) for distributed optimization. As shown by Theorem 2, the alternative approach preserves the essential theoretical guarantees.

3.3 The Riemannian Staircase Algorithm

In typical CSLAM scenarios, the problem dimension can be quite large (e.g., $d \times n > 10^4$), and thus it is often infeasible to solve Problems 3 and 4 with interior-point methods. To address this issue, Burer and Monteiro in their seminal work [11] propose to solve *rank-restricted* versions of the original SDPs. This approach is justified by a theorem of Barvinok [36] and Pataki [37], which guarantees the existence of *low-rank* solutions for SDPs with compact search spaces. Specifically, applying this theorem to Problem 3 and 5 guarantees that both SDPs admit solutions with rank no greater than $(d + 1)\sqrt{n} \ll dn$ [10]. As a direct consequence of Theorem 1, we show that the same result holds for our non-compact SDP (Problem 4).

Corollary 1. Problem 4 admits a minimizer Z_T^* with $\text{rank}(Z_T^*) \leq (d + 1)\sqrt{n}$.

For SDPs with block-diagonal constraints, Boumal [10] extends the general approach of Burer and Monteiro [11] by further exploiting the *geometric* structure within the problem. The result is an elegant algorithm known as the *Riemannian Staircase*, which has been used as the back-end SDP solver in [5, 6]. In the Riemannian Staircase, we search for the optimal solution to SDP by solving a hierarchy of rank-restricted surrogates. At each level, we impose a rank- r factorization ($r \geq d$) of the original SDP variable, i.e., by letting,

$$Z_R = Y^\top Y, \quad Y = \begin{bmatrix} Y_1 & \dots & Y_n \end{bmatrix} \in \mathbb{R}^{r \times dn}, \quad (14)$$

$$Z_T = X^\top X, \quad X = \begin{bmatrix} X_1 & \dots & X_n \end{bmatrix} \in \mathbb{R}^{r \times (n+dn)}, \quad (15)$$

in Problems 3 and 4, respectively. It can be shown that the resulting rank-restricted SDPs are smooth (albeit non-convex) optimization problems on the Cartesian product of Stiefel manifolds; see Problems 6 and 7 below.

Problem 6 (Rank-restricted SDP for Rotation Synchronization).

$$\underset{Y \in \text{St}(d,r)^n}{\text{minimize}} \quad \text{tr}(Q_R Y^\top Y). \quad (16)$$

Problem 7 (Rank-restricted SDP for Pose Synchronization).

$$\underset{X \in (\text{St}(d,r) \times \mathbb{R}^r)^n}{\text{minimize}} \quad \text{tr}(Q_T X^\top X). \quad (17)$$

In principle, one may attempt to solve Problems 6 and 7 via Riemannian local search algorithms. Due to the non-convex constraints in both problems, however, there is no *a priori* guarantee that the obtained solution is a global minimizer, or that it can be used to extract the SDP solution, at least for small values of r .¹ Nevertheless, given any first-order critical point, we can obtain a *post-hoc* certificate of global optimality by verifying the KKT conditions of the original SDP [10]. We discuss the details of this verification procedure in Section 6.2.

Algorithm 1 summarizes the Riemannian Staircase algorithm for pose synchronization. At level r of the hierarchy, we first solve the rank-restricted SDP using a local search algorithm (line 2). If the obtained first-order solution passes the verification procedure, we use it to extract the solution to SDP and the algorithm terminates (line 3). If not, the current solution is used to warm-start the local search at the next level of the hierarchy (line 5). Although Riemannian Staircase is an iterative procedure, in practice it typically identifies the SDP solution at the first level (e.g., with $r_0 = 5$); see the experiments (Section 7) and [5, 6].

4 Riemannian Block-Coordinate Descent

In this section, we propose a *distributed* local search algorithm to find first-order critical points of the rank-restricted SDPs inside the Riemannian Staircase framework. In both CNL and CSLAM, the cost functions admit a natural *block-separable structure* that breaks the vertices in the pose graph into disjoint partitions $\mathcal{V} \triangleq [n] = \mathcal{B}_1 \uplus \dots \uplus \mathcal{B}_{n_b}$. In CNL, each block corresponds to a single camera, i.e., $n_b = n$ and $\mathcal{B}_i = \{i\}$. In CSLAM, each block corresponds to the trajectory of a single robot α , i.e, n_b is the number of robots and \mathcal{B}_α contains the indices of pose variables owned by robot α . We discuss more complex blocking schemes in Section 4.5.

To exploit the block-separable structure of decision variables and the objective function in such synchronization problems, we propose Riemannian block-coordinate descent (RBCD) as the distributed local search

¹In [38], Boumal et al. show that for almost all SDPs with compact search spaces and linearly independent constraints, if $r(r+1) > 2m$ where m is the number of SDP constraints, any second-order critical points of the corresponding rank-restricted SDPs are globally optimal. We note that this result does not cover Problem 4, since the search space is not compact. In addition, the bound on r (which translates to $r > O(d\sqrt{n})$) is too conservative for typical PGO problems, as in practice global optimality often holds for much smaller r ; see Section 7 and [5, 6].

Algorithm 1 RIEMANNIAN STAIRCASE FOR POSE SYNCHRONIZATION

Input:

- Initial rank $r_0 \geq d$.
- Initial estimate $X \in (\text{St}(d, r_0) \times \mathbb{R}_0^+)^n$ (Section 6.1).

Output:

- Global minimizer X^* of Problem 7 with a corresponding solution $Z_T^* = X^{*\top} X^*$ to Problem 4.
- 1: **for** $r = r_0, \dots, n + dn$ **do**
 - 2: Starting at X , apply distributed local search (Section 4) to find a first-order critical point X^* for Problem 7.
 - 3: **if** X^* passes verification (Section 6.2) **then return** X^* .
 - 4: **else**
 - 5: Set $X \leftarrow \begin{bmatrix} X^* \\ 0_{1 \times (n+dn)} \end{bmatrix}$.
 - 6: **end if**
 - 7: **end for**
-

algorithm within the Riemannian Staircase framework for solving Problems 6 and 7. At an abstract level, RBCD solves a general optimization problem over the direct product of matrix submanifolds,

$$\underset{x \in \mathcal{M}}{\text{minimize}} \quad f(x), \quad \mathcal{M} \triangleq \mathcal{M}_1 \times \dots \times \mathcal{M}_n. \quad (18)$$

Given a disjoint partitioning of indices $[n] = \mathcal{B}_1 \uplus \dots \uplus \mathcal{B}_{n_b}$, each iteration of RBCD optimizes variables in a single block $b \in [n_b]$. For now, this means that in each iteration only a single agent (camera/robot in the context of CNL/CSLAM) updates its decision variables, while other agents do nothing. We address this limitation in Section 4.5 by providing highly effective parallel execution schemes for RBCD. Algorithm 2 provides the pseudocode for RBCD.

The rest of this section is organized to discuss details of each step in Algorithm 2. We begin with the discussion of *block selection rules* in Section 4.1 to determine how blocks should be selected at each iteration of RBCD (Line 2). Then, in Section 4.2, we propose a general *block update rule* for an arbitrary manifold optimization problem. In Section 4.3-4.4, we focus on the special cases of rotation and pose synchronizations in CNL, and derive *optimal* block update rules in these contexts. Finally, in Section 4.5, we discuss parallel execution schemes that further accelerate RBCD in practice.

Algorithm 2 RIEMANNIAN BLOCK-COORDINATE DESCENT (RBCD)

Input:

- Global cost function $f : \mathcal{M} \triangleq \mathcal{M}_1 \times \dots \times \mathcal{M}_n \rightarrow \mathbb{R}$.
- Blocks $[n] = \mathcal{B}_1 \uplus \dots \uplus \mathcal{B}_{n_b}$.
- Initial solution $x^0 \in \mathcal{M}$ (Section 6.1).

Output:

- First-order critical point x^* .
- 1: **for** $t = 0, 1, \dots$ **do**
 - 2: Select block $b \in [n_b]$ with x_b denoting the corresponding component in x .
 - 3: Update x_b by (approximately) solving $x_b^{t+1} \in \text{argmin}_{x_b} f_b(x_b)$ s.t. $x_b \in \mathcal{M}_b$.
 - 4: Carry over all other blocks $x_{b'}^{t+1} = x_{b'}^t, \forall b' \neq b$.
 - 5: **end for**
-

4.1 Block Selection Rules

In this section, we describe three mechanisms for selecting which blocks to update at each iteration of RBCD (line 2). The first two block selection rules are based on random sampling [39, 32]. At each iteration, a block $b \in [n_b]$ is selected with probability p_b . The simplest among such rules is *uniform sampling*, in which all blocks are selected with an equal probability, i.e., $p_b = 1/n_b, \forall b \in [n_b]$.

In practice, it is often the case that selecting certain blocks leads to significantly larger decrement of the cost function compared to others. Therefore, it is natural to assign these blocks higher weights during the sampling process. We refer to this block selection rule as *importance sampling*. In this work, we design the probability of selecting each block to be proportional to the squared norm of Riemannian gradient, i.e., $p_b \propto \|\text{grad}_{x_b} f\|^2, \forall b \in [n_b]$. Under Lipschitz-type conditions, it can be shown that the squared gradient norm provides a lower bound on the cost decrement along the direction of negative gradient [23].

We can also modify importance sampling into a deterministic strategy. At each iteration, we can directly choose the block with the largest squared gradient norm, i.e., $b \in \arg \max \|\text{grad}_{x_b} f\|^2$. We refer to this strategy as *greedy selection* and more specifically the *Gauss-Southwell (GS)* rule [23]. Recent works also propose other variants of greedy selection such as Gauss-Southwell-Lipschitz (GSL) and Gauss-Southwell-Quadratic (GSQ) [23]. However, such rules require additional knowledge about the block Lipschitz constants that are often hard to obtain in practice. For this reason, we restrict our deterministic selection rule to GS. Despite its simpler nature, empirically the GS rule already demonstrates satisfactory performance; see Section 7.

In practice, although importance sampling and greedy selection tend to produce more effective iterations, they also incur additional coordination and communication overhead in the distributed scenario. For example, with greedy selection, at the beginning of each iteration agents need to coordinate and find the block with maximum squared gradient norm. In contrast, uniform sampling incurs minimal overhead in the block selection stage.

4.2 Block update with Riemannian Trust-Region (RTR)

In this section, we describe our default method to perform block update at each iteration of RBCD (line 3). Let $x_b \in \mathcal{M}_b$ be the component of x corresponding to the selected block, and let \hat{x}_c be the complement of x_b in x whose values are fixed at this iteration. Define the *reduced* cost function $f_b : \mathcal{M}_b \rightarrow \mathbb{R}$ as $f_b(x_b) \triangleq f(x_b, \hat{x}_c)$. To perform block update, we solve the reduced problem,

$$\underset{x_b \in \mathcal{M}_b}{\text{minimize}} \quad f_b(x_b). \quad (19)$$

As concrete examples, consider solving the rank-restricted SDP of rotation synchronization (Problem 6) in the context of CSLAM. Recall that in this case, each block $Y_\alpha = \begin{bmatrix} Y_1^\alpha & \dots & Y_{n_\alpha}^\alpha \end{bmatrix} \in \text{St}(d, r)^{n_\alpha}$ corresponds to variables owned by robot α in Problem 6. Fixing all other robots' variables $Y_\beta = \hat{Y}_\beta$, it can be shown that the reduced problem defined over Y_α is of the form,

$$\underset{Y_\alpha \in \text{St}(d, r)^{n_\alpha}}{\text{minimize}} \quad \langle Q_{R[\alpha, \alpha]}, Y_\alpha^\top Y_\alpha \rangle + 2\langle G_\alpha, Y_\alpha \rangle + \text{const}, \quad (20)$$

where $Q_{R[\alpha, \alpha]} \in \mathbb{S}_{\geq 0}^{dn_\alpha}$ is the submatrix of Q_R formed with the rows and columns that correspond to robot α 's variables, and $G_\alpha \in \mathbb{R}^{d \times dn_\alpha}$ is a constant matrix that depends on the (fixed) public variables of robot α 's neighbors.

Similarly, in the case of full pose synchronization (Problem 7), let $X_\alpha = \begin{bmatrix} X_1^\alpha & \dots & X_{n_\alpha}^\alpha \end{bmatrix} \in (\text{St}(d, r) \times \mathbb{R}^r)^{n_\alpha}$ be the set of variables corresponding to the trajectory of robot α . Fixing the variables of all other robots, the reduced problem over X_α is of the form,

$$\underset{X_\alpha \in (\text{St}(d, r) \times \mathbb{R}^r)^{n_\alpha}}{\text{minimize}} \quad \langle Q_{T[\alpha, \alpha]}, X_\alpha^\top X_\alpha \rangle + 2\langle F_\alpha, X_\alpha \rangle + \text{const}, \quad (21)$$

where the constant matrices $Q_{T[\alpha, \alpha]} \in \mathbb{S}_{\geq 0}^{n_\alpha + dn_\alpha}$, $F_\alpha \in \mathbb{R}^{d \times (n_\alpha + dn_\alpha)}$ have similar interpretations as in (20).

The general problem (19) and its particular instances (20) and (21) only involve local variables of each block, and thus can be (locally) solved independently by agent α (after receiving the fixed public variables of its neighbors over the network). Nevertheless, due to the manifold constraints, these problems are in general non-convex and thus hard to solve to global optimality.

A natural alternative is to perform *inexact* update to x_b in order to sufficiently decrease the reduced cost. For this purpose, there is a variety of optimization algorithms on matrix manifolds that one can consider. In this work, we select the popular second-order Riemannian trust-region (RTR) algorithm [13, Chapter 7] to solve the reduced problems. Compared to alternative first-order methods such as Riemannian gradient descent, RTR uses second-order information of the (local) reduced problem to speed up optimization. Empirically, we observe that in most cases a single iteration of RTR yields sufficient descent on the cost function. As mentioned above, since by design each block corresponds to the decision variables of a single agent, RTR iterations (within RBCD) are executed *locally* by the selected agent. More details and extensive analysis of the algorithm are provided in Section 5.

Accelerating RTR via Preconditioning. In practice, most instances of (20) and (21) in CSLAM are poorly conditioned, i.e., the condition numbers of $Q_{R[\alpha,\alpha]}$ and $Q_{T[\alpha,\alpha]}$ are quite large. In these cases, suitable preconditioning can significantly speed up numerical optimization. In general, a Riemannian preconditioner for the reduced problem $\text{Precon } f_b(x_b) : T_{x_b}\mathcal{M}_b \rightarrow T_{x_b}\mathcal{M}_b$ is a linear, symmetric, and positive definite operator that approximates the inverse of the Riemannian Hessian. In the particular cases of SLAM, prior works [40, 6] have already proposed empirically effective preconditioners for problems similar in nature to (20) and (21).² The main idea is to approximate the directional derivatives of the Riemannian gradient with that of the Euclidean gradient in the ambient space. More specifically, we let our preconditioners be,

$$\text{Precon } f(Y_\alpha) : \dot{Y}_\alpha \mapsto \text{Proj}_{T_{Y_\alpha}}(\dot{Y}_\alpha(Q_{R[\alpha,\alpha]} + \lambda I)^{-1}), \quad (22)$$

$$\text{Precon } f(X_\alpha) : \dot{X}_\alpha \mapsto \text{Proj}_{T_{X_\alpha}}(\dot{X}_\alpha(Q_{T[\alpha,\alpha]} + \lambda I)^{-1}), \quad (23)$$

for problem (20) and (21), respectively. The small constant $\lambda > 0$ ensures that the proposed preconditioners are positive definite. It is straightforward to verify that (22) and (23) are linear and symmetric (e.g., see [6, Appendix VI]). In practice, each robot can compute and reuse the Cholesky decomposition of $Q_{R[\alpha,\alpha]} + \lambda I$ and $Q_{T[\alpha,\alpha]} + \lambda I$ for improved numerical efficiency.

4.3 Optimal Update for Single Rotation

The RTR-based block update described in the previous section works for arbitrary instances of the reduced problem (19). Nevertheless, for Problem 6 in CNL, it is possible to perform *optimal* update by optimizing each reduced problem *exactly*. Recall that in CNL, each block in Problem 6 contains a single variable $Y_i \in \text{St}(d, r)$ that corresponds to the “lifted” rotation of a single camera. After fixing all other variables $Y_j = \hat{Y}_j$ for $j \neq i$, the reduced problem over Y_i is,

$$\underset{Y_i \in \text{St}(d,r)}{\text{minimize}} \quad \sum_{j \in N_{\text{out}}(i)} \kappa_{ij} \|\hat{Y}_j - Y_i \tilde{R}_{ij}\|_F^2 + \sum_{k \in N_{\text{in}}(i)} \kappa_{ki} \|Y_i - \hat{Y}_k \tilde{R}_{ki}\|_F^2, \quad (24)$$

where N_{out} and N_{in} distinguish neighbors of i in the pose graph based on edge orientations.

Problem (24) is similar to an instance of the single rotation averaging problem [16]. After a series of algebraic manipulations [33], one can show that (24) is equivalent to minimizing the cost function $\|Y_i - G_i\|_F^2$ for a constant matrix G_i defined as,

$$G_i \triangleq \sum_{j \in N_{\text{out}}(i)} \kappa_{ij} \hat{Y}_j \tilde{R}_{ij}^\top + \sum_{k \in N_{\text{in}}(i)} \kappa_{ki} \hat{Y}_k \tilde{R}_{ki}. \quad (25)$$

Thus the solution to this problem is given by,

$$Y_i^* = \text{Proj}_{\text{St}(d,r)}(G_i), \quad (26)$$

²The only difference is the additional linear terms in our cost functions, as a result of anchoring variables owned by other robots.

where the projection to Stiefel manifold can be implemented in closed-form via singular value decomposition (SVD). Specifically, let $G_i = U_i \Sigma_i V_i^\top$ be a (thin) rank- d SVD of G_i , i.e., $U_i \in \text{St}(d, r)$ and $V_i \in \text{O}(d)$. Then, the projection is simply given by $Y_i^* = U_i V_i^\top$ ([41, Theorem 2.1]). Equation (26) thus gives the optimal block update rule for a single lifted rotation.

4.4 Optimal Update for Single Pose

Similarly, we show that optimal update can be derived for Problem 7 in CNL. Similar to the previous section, each block contains a single variable $X_i = \begin{bmatrix} Y_i & p_i \end{bmatrix} \in \text{St}(d, r) \times \mathbb{R}^r$ corresponding to the “lifted” pose of a single camera. After fixing all other blocks $X_j = \hat{X}_j, \forall j \neq i$, the reduced optimization problem over X_i is,

$$\begin{aligned} & \underset{Y_i, p_i}{\text{minimize}} && \sum_{j \in \text{N}_{\text{out}}(i)} \kappa_{ij} \|\hat{Y}_j - Y_i \tilde{R}_{ij}\|_F^2 + \tau_{ij} \|\hat{p}_j - p_i - Y_i \tilde{t}_{ij}\|_2^2 + \\ & && \sum_{k \in \text{N}_{\text{in}}(i)} \kappa_{ki} \|Y_i - \hat{Y}_k \tilde{R}_{ki}\|_F^2 + \tau_{ki} \|p_i - \hat{p}_k - \hat{Y}_k \tilde{t}_{ki}\|_2^2, \\ & \text{subject to} && Y_i \in \text{St}(d, r), p_i \in \mathbb{R}^r. \end{aligned} \quad (27)$$

In (27), the optimization with respect to $p_i \in \mathbb{R}^r$ is an (unconstrained) linear least squares problem. We can thus analytically eliminate p_i from (27) and form a further reduced problem involving only Y_i . Specifically, given any value of Y_i , the optimal value of p_i (as a function of Y_i) corresponds to the following weighted average in \mathbb{R}^r ,

$$p_i^*(Y_i) = \frac{1}{\tau_i} \left[\sum_{j \in \text{N}_{\text{out}}(i)} \tau_{ij} (\hat{p}_j - Y_i \tilde{t}_{ij}) + \sum_{k \in \text{N}_{\text{in}}(i)} \tau_{ki} (\hat{p}_k + \hat{Y}_k \tilde{t}_{ki}) \right]. \quad (28)$$

$$\tau_i \triangleq \sum_{j \in \text{N}_{\text{out}}(i)} \tau_{ij} + \sum_{k \in \text{N}_{\text{in}}(i)} \tau_{ki}. \quad (29)$$

To derive the reduced problem over Y_i , we substitute (28) into the original cost function (27). After a series of algebraic manipulations, we can show that the resulting problem involves minimizing $\|Y_i - \tilde{G}_i\|_F^2$ where the constant matrix \tilde{G}_i is defined as,

$$\tilde{G}_i \triangleq G_i + \sum_{j \in \text{N}_{\text{out}}(i)} \tau_{ij} \hat{p}_j \tilde{t}_{ij}^\top - \frac{1}{\tau_i} \left[\sum_{j \in \text{N}_{\text{out}}(i)} \tau_{ij} \hat{p}_j + \sum_{k \in \text{N}_{\text{in}}(i)} (\tau_{ki} \hat{p}_k + \hat{Y}_k \tilde{t}_{ki}) \right] \left[\sum_{j \in \text{N}_{\text{out}}(i)} \tau_{ij} \tilde{t}_{ij} \right]^\top. \quad (30)$$

In (30), G_i is the same cost matrix as defined in (25), and the remaining terms summarize costs introduced by the translation measurements. Similar to Section 4.3, the optimal Y_i^* is given by the projection,

$$Y_i^* = \text{Proj}_{\text{St}(d, r)}(\tilde{G}_i). \quad (31)$$

Afterwards, the optimal p_i^* is recovered by substituting Y_i^* into (28).

4.5 Parallel Execution

So far we have assumed that the decision variables are partitioned into (disjoint) blocks $[n] = \mathcal{B}_1 \uplus \dots \uplus \mathcal{B}_{n_b}$ based on agents, and that only one agent updates its block at a time while others remain idle. However, the natural graphical decomposition of objectives in synchronization problems (16) and (17) (inherited from Problems 1 and 2, respectively) allows us to update *multiple* blocks in *parallel* provided that every pair of those blocks are disconnected in the graphical representation. For example, in CNL a subset of cameras can be updated in parallel and independently if there are no inter-camera measurements connecting a camera pair. Similarly, in CSLAM a subset of trajectories (corresponding to multiple robots) can be updated in parallel if there are no inter-robot loop closures between them.

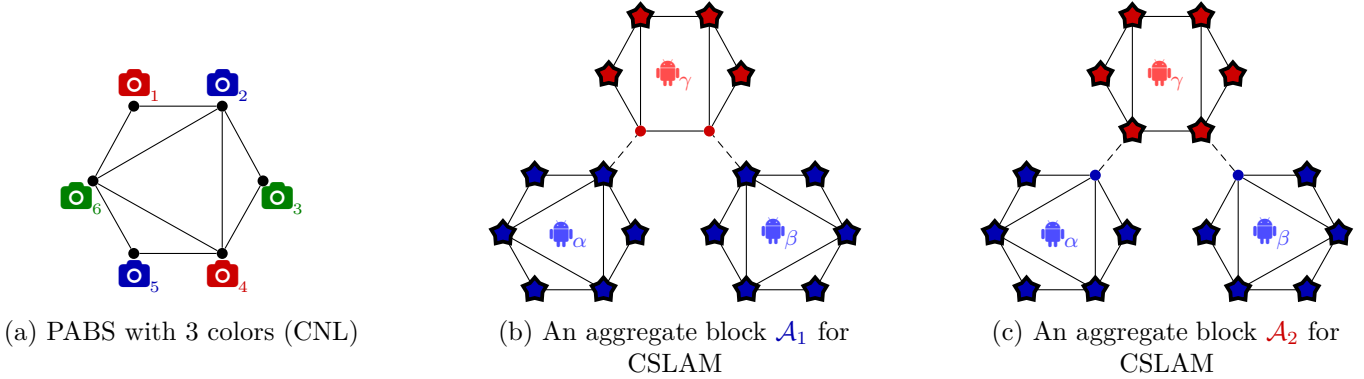


Figure 3: Illustrating PABS (Definition 2) for CNL and CSLAM. (a) A 3-coloring of CNL. The corresponding PABS consists of three aggregate blocks associated to each color, i.e., $\mathcal{S}_{\text{CNL}} = \{\mathcal{A}_1, \mathcal{A}_2, \mathcal{A}_3\}$ where $\mathcal{A}_1 = \{\text{red}_1, \text{red}_4\}$, $\mathcal{A}_2 = \{\text{blue}_2, \text{blue}_5\}$, and $\mathcal{A}_3 = \{\text{green}_3, \text{green}_6\}$. In each iteration of RBCD, one aggregate block \mathcal{A} is selected from \mathcal{S}_{CNL} and the corresponding blocks in \mathcal{A} are updated independently and in parallel. (b) and (c) illustrate two aggregate blocks in a PABS for CSLAM. First, robots are colored with two colors. Then $\mathcal{S}_{\text{CSLAM}} = \{\mathcal{A}_1, \mathcal{A}_2\}$ is a PABS where each aggregate block consists of the “star” nodes. Note that the two aggregate blocks in this PABS have a non-empty overlap.

Definition 2 (Proper Aggregate Blocking Scheme). Let $\mathcal{B} \triangleq \{\mathcal{B}_i\}_{i=1}^{n_b}$. We call $\mathcal{S} \subseteq 2^{\mathcal{B}}$ a *proper aggregate blocking scheme* (PABS) if and only if the following conditions hold.

1. Independence Condition: for all aggregate blocks $\mathcal{A} \in \mathcal{S}$ and every $\mathcal{B}_i, \mathcal{B}_j \in \mathcal{A}$, the vertices in \mathcal{B}_i are disconnected from the vertices in \mathcal{B}_j .
2. Covering Condition: for all vertex $v \in [n]$, there exists at least an aggregate block $\mathcal{A} \in \mathcal{S}$ such that $v \in \bigcup_{\mathcal{B}_i \in \mathcal{A}} \mathcal{B}_i$.

Now suppose \mathcal{S} is a given PABS. Instead of directly sampling individual blocks (Section 4.1), one can slightly modify Algorithm 2 by using similar selection rules to select an *aggregate block* $\mathcal{A} \in \mathcal{S}$ at each iteration of the algorithm. The independence condition implies that the each block $\mathcal{B}_i \in \mathcal{A}$ can be updated in parallel and independently from other blocks $\mathcal{B}_j \in \mathcal{A}$ ($j \neq i$). The covering condition ensures that every node gets a chance to update eventually, provided that aggregate blocks are selected with non-zero probabilities; needless to say, this is necessary for establishing convergence to first-order critical points (Section 5).

It remains to explain how one can design a PABS. Using independent sets to parallelize Gauss-Seidel-type updates is a classical idea known as red-black coloring and, more generally, multicoloring schemes [22]. This is often done by finding a coloring of variables (vertices of the so-called *dependency graph*) such that dependent variables (adjacent vertices) have different colors. We use a similar coloring scheme by exploiting the graphical structure of our problems to design PABS in the context of CNL and CSLAM. The details are provided below.

1. For CNL, we find a valid coloring for cameras such that adjacent cameras have different colors. Each aggregate block \mathcal{A} is then the set of cameras with the same color.
2. For CSLAM, we first find a coloring for the set of *robots* such that *adjacent robots* have different colors.³ Now for each color, we will have an aggregate block consisting of the entire trajectories of all robots with that color, plus the *private* variables of all other robots (see Figure 2b and Definition 1). Figures 3b and 3c illustrate two aggregate blocks for a toy problem.

It is easy to check that the abovementioned schemes are PABS for CNL and CSLAM. The PABS proposed for CSLAM is slightly more complex than the coloring-based PABS proposed for CNL mainly due to the larger size of CSLAM problems.

³Two robots are “adjacent” if there is an inter-robot loop closure connecting their trajectories.

Finding a vertex coloring with the smallest number of colors is an NP-hard problem. Nonetheless, there are simple greedy approximation algorithms that can color graph vertices with at most $\Delta + 1$ colors where Δ is the maximum degree of the (agent-level) dependency graph. In the case of CSLAM/CNL, Δ is the maximum number of robots/camera adjacent to one robot/camera. Consequently, in many applications Δ is often bounded by a constant due to the sparse nature of these problems. In practice, $(\Delta + 1)$ -coloring schemes can be obtained through collaboration; see [42, 43] and references therein for distributed coloring algorithms.

5 Convergence Analysis for RBCD

In this section, we formally establish convergence guarantees for RBCD (Algorithm 2). Under a generalized Lipschitz-type condition for the Riemannian gradient, we show that RBCD converges to first-order critical points with *global* sublinear convergence rate. In particular, we show that the required conditions hold in CNL and CSLAM, and thus RBCD achieves the stated global convergence rate in these applications. Our analysis in this section generalizes straightforwardly to more sophisticated blocking schemes (Section 4.5). Specifically, the global convergence rate (Theorem 3) would still hold after modifying certain constants in the rate estimates.

As preliminaries to the main technical results, we introduce two definitions that play important roles in our subsequent analysis. First, to analyze RBCD with the greedy selection rule (Section 4.1), we work with the *maximum block norm* [23] defined below.

Definition 3 (Maximum Block Norm). Given a tangent vector $\eta \in T_x\mathcal{M}$ and a disjoint partitioning of the indices $[n] = \mathcal{B}_1 \uplus \dots \uplus \mathcal{B}_{n_b}$, let η_b denote the component of η that corresponds to block $b \in [n_b]$. The *maximum block norm* of η is defined as,

$$\|\eta\|_{\mathcal{B}} \triangleq \max_{b \in [n_b]} \|\eta_b\|. \quad (32)$$

Intuitively, $\|\eta\|_{\mathcal{B}}$ returns the largest norm among individual blocks of η . Therefore, for any valid partitions, $\|\eta\|_{\mathcal{B}} = 0$ implies η is identically zero.

Another important concept that we will use extensively is the so-called Lipschitz-type gradient for pullbacks [44]. Formally, for a function $f : \mathcal{M} \rightarrow \mathbb{R}$, its *pullback* at $x \in \mathcal{M}$ is defined as,

$$\hat{f}_x \triangleq f \circ \text{Retr}_x : T_x\mathcal{M} \rightarrow \mathbb{R}, \quad (33)$$

where Retr_x is a retraction operator restricted to $T_x\mathcal{M}$ [13]. \hat{f}_x is said to have Lipschitz-type gradient if it satisfies the following condition.

Definition 4 (Lipschitz-type gradient for pullbacks⁴ [44]). There exists a constant $c_g \geq 0$ such that for any $x \in \mathcal{M}$ and $\eta \in T_x\mathcal{M}$,

$$|\hat{f}_x(\eta) - [f(x) + \langle \eta, \text{grad}_x f \rangle]| \leq \frac{c_g}{2} \|\eta\|_2^2. \quad (34)$$

The Lipschitz-type gradient condition given in (34) paves the way for establishing convergence guarantees for a family of local search algorithms on Riemannian manifolds. For example, with (34) it can be shown that the standard Riemannian gradient descent algorithm with fixed step size converges to first-order critical points [44, Theorem 5]. Next, we present the first technical result in this section, which shows that the reduced cost functions in CNL and CSLAM enjoy the favorable property of Lipschitz-type gradient for pullbacks.

Lemma 1. The cost functions in the reduced problems (20), (21), (24), (27) have Lipschitz-type gradients for their respective pullbacks.

⁴We note that Boumal et al. [44] work with a less restrictive version of (34) where the inequality only needs to hold for $\|\eta\| < \rho$ where ρ is a constant. Nevertheless, the more general condition suffices for subsequent analysis.

Next, we show that each iteration of Algorithm 2 yields *sufficient descent* on the global cost function. Our analysis is similar to the one used in proving first-order convergence of RTR [44]. In special cases where exact updates are possible (Sections 4.3-4.4), the corresponding cost decrement will be strictly better and hence convergence is still guaranteed.

To proceed, we briefly review how RTR is used to solve the reduced problem (19). RTR is an iterative algorithm, and each inner iteration solves a so-called *trust-region subproblem* at the current iterate (denoted with a slight abuse of notation as) $x_b \in \mathcal{M}_b$. Each inner iteration uses a quadratic *model function* $\hat{m}_{x_b} : T_{x_b}\mathcal{M}_b \rightarrow \mathbb{R}$ that approximates the local pullback cost $\hat{f}_{x_b} \triangleq f_b \circ \text{Retr}_{x_b}$,

$$\hat{m}_{x_b}(\eta_b) \triangleq f_b(x_b) + \langle \eta_b, \text{grad}_{x_b} f_b \rangle + \frac{1}{2} \langle \eta_b, H[\eta_b] \rangle, \quad (35)$$

where $H : T_{x_b}\mathcal{M}_b \rightarrow T_{x_b}\mathcal{M}_b$ is a user-specified map on the tangent space. For ease of notation, we have omitted the dependence of H on x_b . Given the model function, the trust-region subproblem for this inner iteration is defined as,

$$\underset{\eta_b \in T_{x_b}\mathcal{M}_b}{\text{minimize}} \quad \hat{m}_{x_b}(\eta_b) \quad \text{subject to} \quad \|\eta_b\| \leq \Delta, \quad (36)$$

where $\Delta > 0$ is the current trust-region radius.⁵ After obtaining an (approximate) solution η_b^* to (36), the quality of this solution is checked by forming the following quotient,

$$\rho \triangleq \frac{\hat{f}_{x_b}(0) - \hat{f}_{x_b}(\eta_b^*)}{\hat{m}_{x_b}(0) - \hat{m}_{x_b}(\eta_b^*)}. \quad (37)$$

Intuitively, ρ measures the *agreement* between the actual cost decrement and model decrement. Depending on whether ρ is greater than a user-specified threshold $\rho' \in (0, 1/4)$, the candidate solution is either accepted or rejected, i.e., the next iterate x_b^+ is set to,

$$x_b^+ = \begin{cases} \text{Retr}_{x_b}(\eta_b^*), & \text{if } \rho > \rho', \\ x_b, & \text{otherwise.} \end{cases} \quad (38)$$

At the same time, the trust-region radius for the next inner iteration of RTR is adjusted according to,

$$\Delta^+ = \begin{cases} \Delta/4, & \text{if } \rho < 1/4, \\ \min(2\Delta, \bar{\Delta}), & \text{if } \rho > 3/4 \text{ and } \|\eta_b^*\| = \Delta, \\ \Delta, & \text{otherwise.} \end{cases} \quad (39)$$

$\bar{\Delta}$ is a user-specified maximum trust-region radius. See, e.g., [13, Algorithm 10] for the complete pseudocode of RTR. We are now ready to establish sufficient descent for Algorithm 2. Following [44], we make the following standard assumptions.

Assumption 1 (Assumption on reduced cost). In Algorithm 2, the reduced cost function f_b in (19) has Lipschitz-type gradient for pullbacks with Lipschitz constant $c_b \geq 0$, for all $b \in [n_b]$.

We note that this assumption is easily satisfied in practice; see [44, Lemma 2.7]. In particular, Lemma 1 implies that Assumption 1 holds for CNL and CSLAM.

Assumption 2 (Assumptions on RTR). When using RTR to solve the reduced problem (19), we require,

1. The user-specified map H in (35) is globally radially linear, i.e.,

$$H[c\eta_b] = cH[\eta_b], \quad \text{for all } \eta_b \in T_{x_b}\mathcal{M}_b \text{ and } c \geq 0. \quad (40)$$

⁵This is not to be confused with the maximum degree symbol in Section 4.5.

2. H is globally bounded, i.e., there exists $c_0 \geq 0$ such that,

$$\max_{\eta_b \in T_{x_b} \mathcal{M}_b, \|\eta_b\| \leq 1} \langle \eta_b, H[\eta_b] \rangle \leq c_0. \quad (41)$$

3. The initial trust-region radius, denoted as Δ_0 , is bounded away from zero by,

$$\Delta_0 \geq \lambda_b \|\text{grad}_{x_b} f_b\|, \quad (42)$$

where x_b is the initial value of the selected block b (i.e., before the first inner iteration of RTR) and λ_b is a block-specific constant defined as,

$$\lambda_b \triangleq \frac{1}{8(c_b + c_0)}. \quad (43)$$

Our requirements on RTR are particularly lax; see also [44, Assumption 3.4]. The simplest choice of H that satisfies the first two regularity conditions in Assumption 2 is the identity map. In our implementation, we use the Riemannian Hessian for faster convergence. It is known that for smooth cost functions over compact manifolds, the Riemannian Hessian satisfies the required regularity conditions [13, Corollary 7.4.6]. We leave the extension of this result to product manifolds with Euclidean spaces for future work. Finally, the last condition in Assumption 2 can be easily satisfied by using a sufficiently large initial trust-region radius.

Lemma 2 (Sufficient descent in Algorithm 2). Let x^t be the solution of Algorithm 2 after t iterations, and $b_t \in [n_b]$ the selected block for the next iteration. Under Assumption 1 and 2, the next iteration of Algorithm 2 reduces the global cost function by *at least*,

$$f(x^t) - f(x^{t+1}) \geq \frac{1}{4} \lambda_{b_t} \|\text{grad}_{x_{b_t}^t} f\|^2, \quad (44)$$

where λ_{b_t} is the block-specific constant corresponding to block b_t defined in (43).

With Lemma 2, we now prove the main theorem of this section, which establishes the *global* sublinear convergence of RBCD for general manifold optimization problems.

Theorem 3 (Global convergence rate of Algorithm 2). Let f^* denote the global minimum of the optimization problem (18), x^0, x^1, \dots, x^{T-1} denote the iterates of Algorithm 2, and $b_0, b_1, \dots, b_{T-1} \in [n_b]$ denote the corresponding blocks selected at each iteration. Under Assumption 1 and 2, Algorithm 2 with *uniform sampling* or *importance sampling* yields the following guarantees,

$$\min_{0 \leq t \leq T-1} \mathbb{E}_{b_{0:t-1}} \|\text{grad}_{x^t} f\|^2 \leq \frac{4n_b(f(x^0) - f^*)}{T \cdot \min_{b \in [n_b]} \lambda_b}, \quad (45)$$

In addition, Algorithm 2 with *greedy selection* yields the following guarantee,

$$\min_{0 \leq t \leq T-1} \|\text{grad}_{x^t} f\|_{\mathcal{B}}^2 \leq \frac{4(f(x^0) - f^*)}{T \cdot \min_{b \in [n_b]} \lambda_b}, \quad (46)$$

where $\|\cdot\|_{\mathcal{B}}$ is the maximum block norm in Definition 3.

We conclude this section by presenting the specialized version of Theorem 3 in the case of rotation synchronization and pose synchronization. Since Assumption 1 always holds by Lemma 1, we have the following straightforward corollary.

Corollary 2 (Global convergence rate of Algorithm 2 for Problems 6 and 7). Under Assumption 2, Algorithm 2 using RTR achieves the global convergence rates in Theorem 3 on rank-restricted SDPs for pose and rotation synchronization problems (Problems 6 and 7). The same convergence rates are also achieved with the *optimal* update rules in CNL (Sections 4.3-4.4).

Corollary 2 states that under fairly lax requirements on RTR, RBCD is guaranteed to converge to first-order critical points of the rank-restricted SDPs for CNL and CSLAM. This guarantee validates RBCD as a distributed local search algorithm that can be applied within the Riemannian Staircase framework.

Remark 2. With the parallelism provided by PABS (Section 4.5), we can further improve the global convergence rates of RBCD in Theorem 3. For example, the constant n_b in (45) can be replaced by the number of aggregate blocks in the PABS, which is typically bounded by a small constant (e.g., the maximum degree in the sparse dependency graph); see Section 4.5.

6 Distributed Initialization, Verification, and Rounding

6.1 Distributed Initialization

For centralized SLAM, various initialization methods have been proposed; see [34] and the references therein. In the distributed setting, the simplest technique one can consider is *spanning tree initialization*, in which pose estimates are initialized by propagating noisy measurements along a spanning tree in the pose graph.

Chordal initialization is another popular technique, in which one first relaxes Problem 1 and 2 into linear least squares problems by dropping the non-convex rotation constraints, and subsequently project the solutions to the rotation group. For distributed computation, Choudhary et al. [2] propose to solve the resulting linear least squares problem via distributed iterative methods such as JOR and SOR [22]. In this work, we choose chordal initialization with SOR as the default initialization technique.

6.2 Distributed Verification

So far, we have proposed RBCD as our distributed local search algorithm for identifying first-order critical points of the rank-restricted SDPs at a specific level of the Riemannian Staircase. However, we are interested in recovering an optimal solution to the corresponding SDPs. For example, given a first-order critical point $Y^* \in \text{St}(d, r)^n$ of Problem 6, we want to verify if the tentative solution $Z_R^* = Y^{*\top} Y^*$ indeed solves Problem 3.

The theory of Lagrangian duality makes such verification possible. Specifically, given a first-order critical point $Y^* \in \text{St}(d, r)^n$ to Problem 6, $Z_R^* = Y^{*\top} Y^*$ is an optimal solution to the SDP if and only if the corresponding *dual certificate* matrix $S_R = Q_R - \Lambda_R$ is positive semidefinite; see Theorem 3.3 and Corollary 3.6 in [10]. Here, $\Lambda_R \in \mathbb{R}^{dn \times dn}$ is the $(d \times d)$ -block-diagonal matrix containing the Lagrange multipliers corresponding to the tentative SDP solution Z_R , and admits the closed-form expression $\Lambda_R = \text{SymBlockDiag}_d(Q_R Z_R^*)$.

Similar result extends to the case of pose synchronization. Given a first-order critical point $X^* \in (\text{St}(d, r) \times \mathbb{R}^r)^n$ to Problem 7, $Z_T^* = X^{*\top} X^*$ is an optimal solution to Problem 4 if and only if the corresponding dual certificate $S_T = Q_T - \Lambda_T$ is positive semidefinite. In this case, the Lagrange multipliers Λ_T can be recovered via a similar closed-form expression; see [6, Appendix VIII].

In summary, the verification procedure for both rotation synchronization and pose synchronization boils down to checking that the corresponding dual certificate matrix has nonnegative minimum eigenvalue. In the centralized setting, Rosen and Carlone [40] propose to do this via the Lanczos algorithm with spectrum shifting. In the distributed regime, the Lanczos algorithm can be replaced by distributed eigenvalue solvers such as [45]. Since both S_R and S_T inherit the favorable graphical structure from the original connection Laplacians Q_R and Q_T , the execution of these algorithms only requires *local* communications (e.g., to compute any matrix vector products). Still, we note that with the typical noise level that we encounter in practical situations, Riemannian Staircase usually terminates at the first level (e.g., with $r_0 = 5$, see Section 7) and thus verification can be treated as an optional step.

In the undesirable situations where verification fails (i.e., the algorithm converges to a saddle point or local minimum of the rank-restricted SDP), the eigenvector corresponding to the negative eigenvalue of the dual certificate can be used to construct a descent direction at the next level of the Riemannian Staircase (see [10, Corollary 3.10] and [6, Appendix IX]), which allows the algorithm to escape the local minimum and continue to search for the SDP solution.

6.3 Distributed Rounding

After solving the SDP relaxations (Problem 3 and 4), we ultimately need to recover solutions to the original synchronization problems (Problem 1 and 2). In this section, we describe a distributed recovery procedure that is guaranteed to return global minimizers to Problem 1 and 2 provided that the corresponding SDP relaxations are *exact* (see Theorem 2).

For rotation synchronization, let $Z_R^* = Y^{*\top} Y^*$ be a solution to Problem 3, where $Y^* = [Y_1^* \ \dots \ Y_n^*] \in \text{St}(d, r)^n$. If the SDP relaxation is exact, the first $d \times dn$ block row of the solution is given by $Z_{R(1:d,:)}^* = [R_1^* \ \dots \ R_n^*]$, where $\{R_i^*\}$ is a global minimizer to Problem 1. From Y^* , we can trivially recover this global minimizer via,

$$R_i^* = Y_1^{*\top} Y_i^*, \forall i \in [n]. \quad (47)$$

Similarly, let $Z_T^* = X^{*\top} X^*$ be a solution to Problem 4, where $X^* = [Y_1^* \ p_1^* \ \dots \ Y_n^* \ p_n^*] \in (\text{St}(d, r) \times \mathbb{R}^r)^n$. By Theorem 2, if the SDP relaxation is exact, the first $d \times (n + dn)$ block row of its solution is given by $Z_{T(1:d,:)}^* = [R_1^* \ t_1^* \ \dots \ R_n^* \ t_n^*]$, where $\{R_i^*, t_i^*\}$ is a global minimizer to Problem 2. In this case, we can recover the rotation variables using the same closed-form expression (47). In addition, we can recover the translation variables via,

$$t_i^* = Y_1^{*\top} p_i^*, \forall i \in [n]. \quad (48)$$

When SDP relaxations are not exact, we augment (47) with an additional projection step that ensures the result is a valid rotation matrix, i.e.,

$$R_i = \text{Proj}_{\text{SO}(d)}(Y_1^{*\top} Y_i^*), \forall i \in [n]. \quad (49)$$

In (49), the projection can be carried out using SVD. While the rounded solutions are no longer guaranteed to be globally optimal, empirically we observe that they frequently remain as good approximate solutions. Lastly, we note that in the distributed setting, the above rounding procedure induces minimal communication overhead. Indeed, to perform (47)-(49), each agent only needs to receive Y_1^* via the network, which is a small $r \times d$ matrix.

7 Experiments

In this section, we perform extensive evaluation of the proposed RBCD algorithm on both CSLAM and CNL problems. By default, we implement the parallel execution schemes discussed in Section 4.5 by optimizing aggregate blocks in each iteration of RBCD. To initialize the local search algorithms, we implement distributed chordal initialization with SOR and flagged initialization [2]. The default relaxation parameter for SOR is set to $\gamma = 1$ as recommended by the authors in [2]. All implementations are written in MATLAB. All experiments are done on a laptop with an Intel Core i7-7700HQ 2.80GHz CPU and 8 GB RAM.

Simulation Setup

We create 3D simulation environments for both CNL and CSLAM problems. For CNL, we simulate a network of cameras arranged in a 3D grid; see Figure 4. With a given measurement probability (default 0.8), each pair of neighboring cameras obtains a noisy measurement of their relative transformation. Similarly, for CSLAM, we simulate a scenario in which multiple robots move next to each other in a 3D grid with lawn mower trajectories; see Figure 5. With a given probability (default 0.3), loop closures are added to connect neighboring poses. For all relative measurements, we simulate Langevin rotation noise with zero mean and standard deviation σ_R , and Gaussian translation noise with zero mean and standard deviation σ_t . The default noise parameters are $\sigma_R = 5^\circ$, $\sigma_t = 0.05m$.

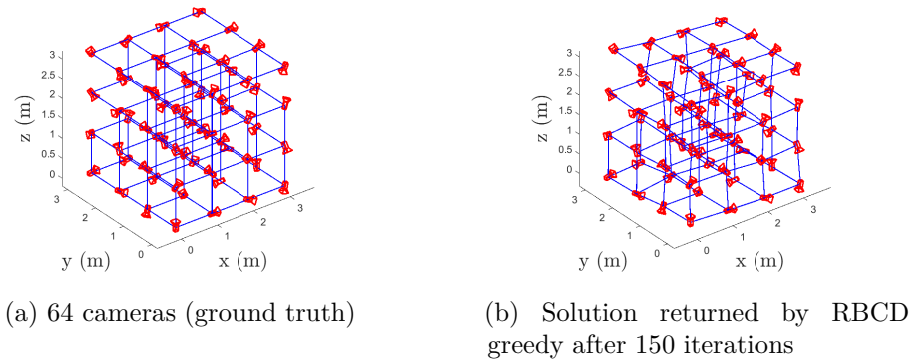


Figure 4: Example CNL simulation. Cameras with random orientations are placed on a 3D grid. Blue edges denote noisy relative measurements.

Performance Metrics

In subsequent experiments, we use the following metrics to assess the quality of a given solution. First, we compute the *optimality gap* $f - f_{\text{SDP}}^*$, where f_{SDP}^* is the optimal value of the centralized SDP relaxation [6]. In general, f_{SDP}^* gives a lower bound on the global minimum of the PGO problem. However, under typical low noise regimes, SDP relaxation is expected to be exact (see Theorem 2), and thus $f_{\text{SDP}}^* = f_{\text{MLE}}^*$ also gives the global minimum of the original maximum likelihood estimation (MLE) problem. In this case, we also compute the rotation and translation *root mean square errors (RMSE)* of the given solution with respect to the global minimizer, using the orbit distance defined in [5, Appendix C.1]. Note that occasionally, we also evaluate RMSE with respect to the ground truth poses. Lastly, to evaluate the quality of local search, we record the *Riemannian gradient norm* $\|\text{grad}_x f\|$, which quantifies how close the given solution is to a first-order critical point.

7.1 CSLAM Experiments

In this section, we evaluate the performance of RBCD on CSLAM problems, and report results on both simulations and existing benchmark datasets. In our experiments, we compare the performance of RBCD against the standard Riemannian gradient descent (RGD) algorithm with Armijo’s backtracking line search (implemented in Manopt [46]), as well as the state-of-the-art distributed PGO solver proposed in [2]. For conciseness, we only report results on pose synchronization, which is the standard problem solved by most SLAM back-ends.

Similar to [2], in most of our results below, we show convergence as a function of iterations rather than runtime.⁶ This is because in the distributed setting, the number of iterations directly determines the communication costs. In addition, we note that each iteration of RGD requires more communication efforts than RBCD, due to the need to perform backtracking line search.

7.1.1 Convergence vs. RGD

In our first set of experiments, we compare the convergence rate of RBCD (Algorithm 2) against the baseline RGD algorithm for solving the rank-restricted SDPs (Problem 7) with $r = 5$. We consider three block selection rules as proposed in Section 4.1: uniform sampling, importance sampling, and greedy selection. Figure 6 shows the result of running all algorithms for 400 iterations in the 4 robot scenario depicted in Figure 5a. All three variants of RBCD clearly outperform RGD in terms of convergence rate. Furthermore, greedy selection and importance sampling are faster compared to uniform sampling, as they prioritize blocks that lead to better

⁶For completeness, we note that as the block size varies between 125 and 1000, the per-iteration runtime of Algorithm 2 (using a single iteration of RTR as implemented in Manopt [46]) varies between 0.05 – 0.3 sec, which is fairly small compared to additional time incurred by network overhead.

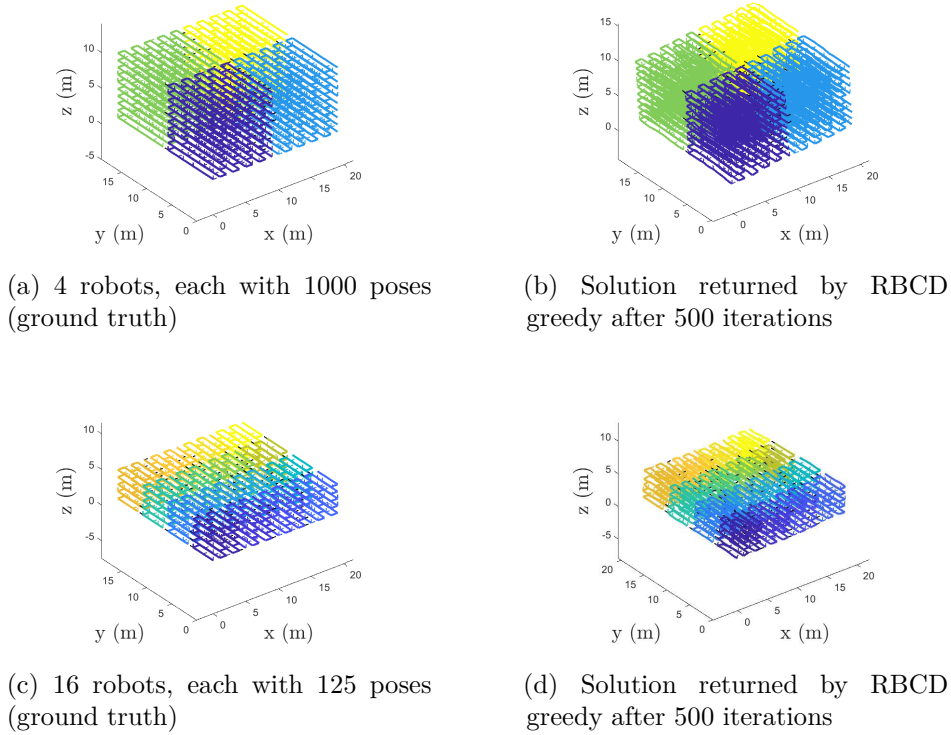


Figure 5: Example CSLAM simulations. Colors denote trajectories of different robots. Solid lines represent robot odometry and dashed lines represent loop closure measurements. Pose orientations are not visualized.

improvements. The final RMSE results (Figure 6c-6d) suggest that the solutions of RBCD are numerically close to the global minimizer, confirming that the solutions are converging to a global minimum.

Similarly, Figure 7 shows the result in the 16 robot scenario depicted in Figure 5c. RBCD again outperform RGD, but convergence is nevertheless slower. Later in this section, we systematically evaluate the scalability of RBCD. In addition, we observe that in both the 4 robot and 16 robot scenarios, RBCD exhibits locally *linear* convergence rate. While this result has been formally proved in the case of spheres ($r = 1$) [32], we leave its extension to the general case of Stiefel manifolds for future work.

7.1.2 Varying Noise Level

In this section, we evaluate RBCD under varying noise levels. We compare our performance against the state-of-the-art distributed PGO solver proposed by Choudhary et al. [2], which uses SOR to solve a single Gauss-Newton iteration. For brevity, we refer to their algorithm as DGN (Distributed Gauss-Newton) in the following experiments. As recommended by the authors, we set the relaxation parameter of SOR to 1 (i.e., Gauss-Seidel) for DGN. Both RBCD and DGN use the same initialization.

Intuitively, as measurement noise increases, local search algorithms face increasing difficulty converging to globally optimal solutions. An example is shown in Figure 8, where the rotation noise is increased to $\sigma_R = 8^\circ$, and translation noise is kept at $\sigma_t = 0.05m$. Both distributed initialization (Figure 8b) and DGN (Figure 8c-8d) produce estimates that are visibly suboptimal compared to the global MLE solution (Figure 8f). For comparison, we run RBCD with greedy selection with $r = 5$ for 500 iterations. Figure 8e shows its solution *after rounding*. The returned solution is visibly more accurate, and the corresponding cost is much closer to the global minimum.

Figure 9 shows a systematic comparison between RBCD and DGN in varying noise regimes. While the original DGN algorithm only performs a single Gauss-Newton update with SOR, we also include the results of using multiple Gauss-Newton updates for a more comprehensive comparison (purple curve in Figure 9).

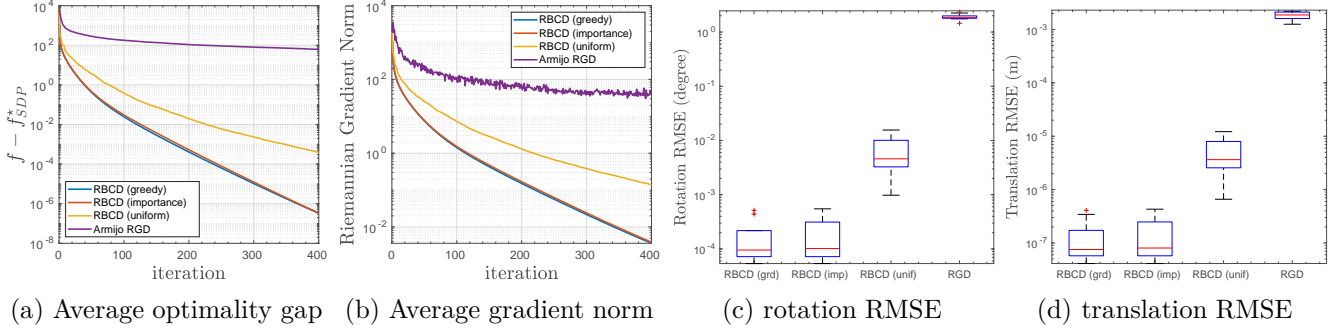


Figure 6: Local search results in the 4 robot scenario (Figure 5a) averaged across 10 random instances. Noise parameters are $\sigma_R = 5^\circ, \sigma_t = 0.05m$. (a) Optimality gap $f - f_{SDP}^*$, (b) Riemannian gradient norm, (c) boxplot of final rotation RMSE with respect to MLE, (d) boxplot of final translation RMSE with respect to MLE.

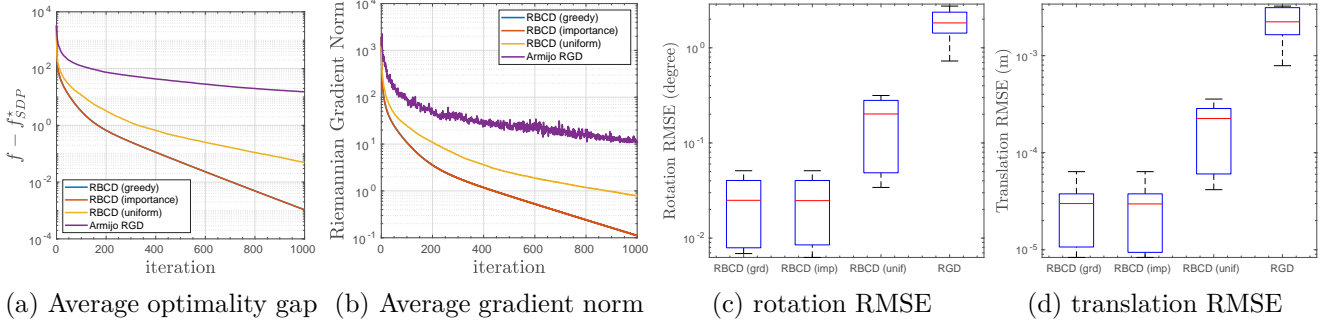


Figure 7: Local search results in the 16 robot scenario (Figure 5c) averaged across 10 random instances. Noise parameters are $\sigma_R = 5^\circ, \sigma_t = 0.05m$. (a) Optimality gap $f - f_{SDP}^*$, (b) Riemannian gradient norm, (c) boxplot of final rotation RMSE with respect to MLE solution in degrees, (d) boxplot of final translation RMSE with respect to MLE solution in meters.

Following [2], we terminate SOR when the change in solution across consecutive iterations is less than a threshold (0.1 and 0.01 in the figure). RBCD is terminated when the Riemannian gradient norm is less than 0.1, and its solution is then rounded to ensure fair comparison. Since the termination conditions are different, we also show the average number of iterations used by each algorithm in Figure 9b.

Under most noise regimes, RBCD produces better solutions compared to DGN while using similar number of iterations. Furthermore, we note that under certain noise threshold (around 11° in the figure), the solutions returned by RBCD are *near-optimal* with an average optimality gap close to 10^{-3} . The optimality gap is not exactly zero since the algorithm is terminated when the Riemannian gradient norm is below 0.1. Nevertheless, as soon as the noise increases above the critical threshold of 11° , RBCD begins to gain nontrivial error, indicating that the algorithm converges to local minima.⁷ In these cases, further rank relaxation and escaping (Section 6.2) is needed to help the algorithm converge to the global minimum.

To complement the above result, Figure 10 reports the convergence speed of RBCD under varying rotation and translation noise, averaged across 10 runs. As rotation noise increases, RBCD requires more iterations to converge to the same precision. Moreover, under high noise (e.g., $\sigma_R = 15^\circ$), the algorithm has more difficulty converging to the global minimum, which is consistent with our earlier observation in Figure 9.

Interestingly, varying translation noise has an *opposite* effect on the convergence speed. As shown in Figure 10b, as translation noise σ_t increases, RBCD takes less iterations to converge, and furthermore always converges to the correct global minimum. This suggests that the real difficulty in pose synchronization lies in the estimation of rotations, which is the source of non-convexity in the problem.

To further illustrate the contradictory effects of σ_R and σ_t , we examine the condition number of the connection Laplacian matrix under varying noise levels. Figure 11 shows averaged condition numbers on a pose

⁷As reference, the centralized SDP relaxation [6] ceases to be exact for this experiment when $\sigma_R = 15^\circ$.

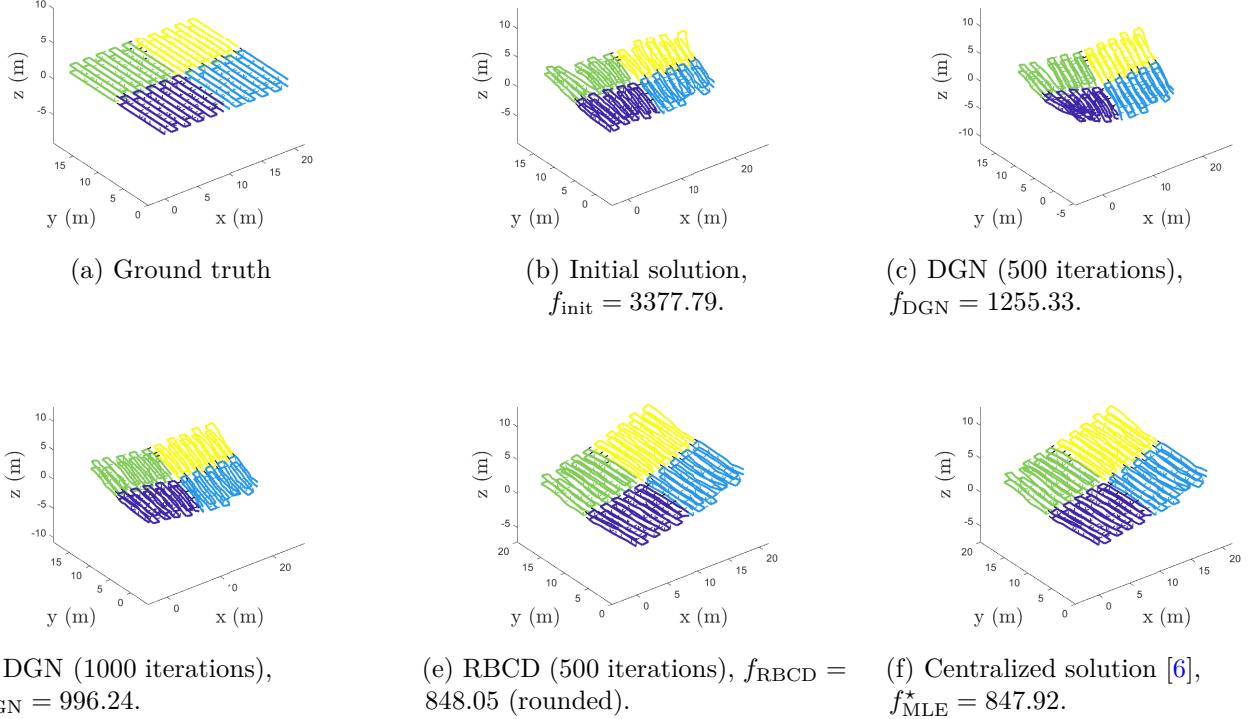


Figure 8: Solutions returned by DGN [2] and the proposed RBCD algorithm in scenario with increased rotation noise ($\sigma_R = 8^\circ$, $\sigma_t = 0.05m$). For each solution, we also record the corresponding final cost. (a) Ground truth (4 robots, each with 200 poses), (b) Distributed chordal initialization with 500 SOR iterations, (c) DGN with 500 SOR iterations, (d) DGN with 1000 SOR iterations, (e) RBCD (greedy selection) with 500 iterations *after rounding*, (f) Globally optimal MLE solution computed with Cartan-Sync [6].

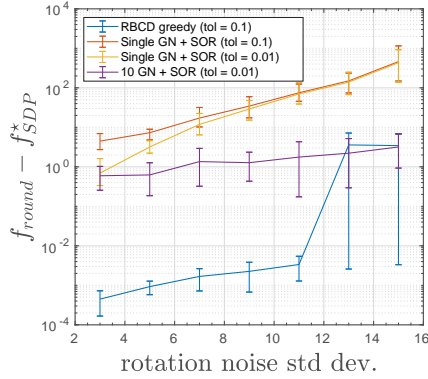
graph with fixed topology and overall loop closure probability of 0.3. As the noise ratio σ_R/σ_t increases (i.e., σ_R increases or σ_t decreases), on average the conditioning becomes worse, indicating that the problem becomes harder to solve numerically. We note that such results are consistent with the performance of RBCD shown in Figure 10.

7.1.3 Varying Number of Robots

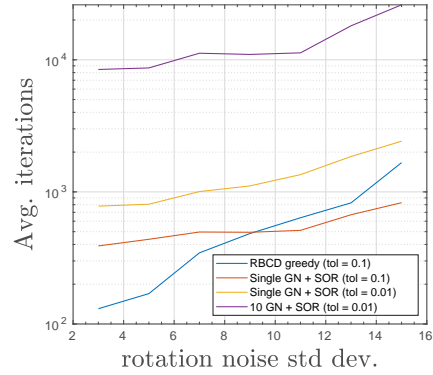
We examine how RBCD scales with respect to the number of robots that participate in CSLAM. For this, we run RBCD with greedy selection with increasing number of robots, where each robot owns 125 poses. The convergence performance averaged across 5 runs is shown in Figure 12. For typical number of robots (less than 20), RBCD converges reasonably fast to *near-optimal* solutions as shown in Figure 12a. Nevertheless, we note that empirical convergence rate is still affected by problem conditioning (e.g., determined by rotation and translation noise as discussed in the previous section).

7.1.4 Varying Inter-robot Connectivity

We also investigate the effect of varying pose graph topologies on the performance of RBCD. The main parameter we vary is the probability of *inter-robot* loop closures, as these are the essential measurements that couple together individual robots' estimation problems. Figure 13 shows results after running 1000 iterations of RBCD (with greedy selection) in a simulated scenario with 16 robots. In this experiment, we fix the probability of *intra-robot* loop closures (i.e., loop closures within a single robot's trajectory) to be 0.1, so that inter-robot loop closures play an essential role for reducing the overall estimation error. Unlike earlier experiments, in this

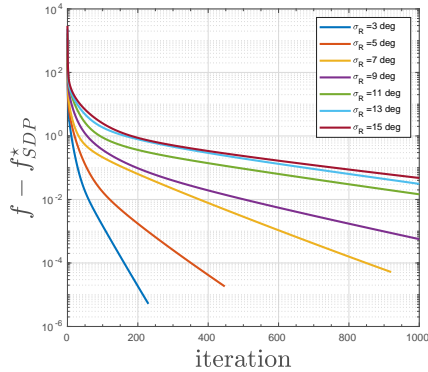


(a) Average optimality gap of final rounded solution.

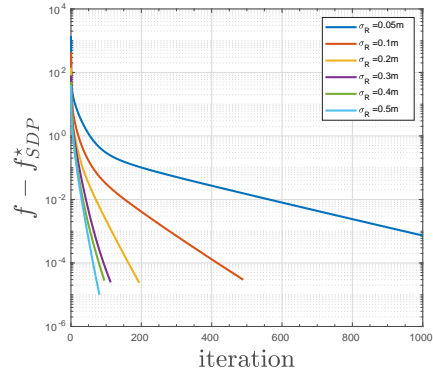


(b) Average number of iterations.

Figure 9: Performance of RBCD and DGN in the 4 robot scenario under increasing rotation noise. Translation noise is fixed at $\sigma_t = 0.1m$. Results are collected in 10 random runs. (a) Average optimality gap *after* rounding, with the error bars denoting the range of optimality gaps across 10 runs; (b) Average number of iterations.



(a) Varying rotation noise



(b) Varying translation noise

Figure 10: Convergence of RBCD with greedy selection in the 4 robots scenario with varying noise levels. Each robot owns 200 poses. Results are averaged across 10 runs. (a) Varying rotation noise σ_R while fixing translation noise $\sigma_t = 0.1m$. (b) Varying translation noise σ_t while fixing rotation noise $\sigma_R = 5^\circ$.

section we evaluate RMSE *with respect to ground truth poses*, in order to show how adding loop closures improve the final estimation quality. As we can see in Figure 13a, as more inter-robot loop closures are added, the overall rotation RMSE decreases monotonically. In addition, Figure 13b shows that as more inter-robot loop closures are added, more poses become public and hence the average communication payloads increase as expected. Still, the maximum amount of data exchange (corresponding to 0.9 inter-robot loop closure probability) is below 30MB, which is fairly lightweight considering that the global pose graph has 2000 poses.

7.1.5 Performance on Benchmark Datasets

To conclude our CSLAM experiments, in this section we report the performance of RBCD on existing 2D and 3D benchmark SLAM datasets. To simulate a collaborative scenario, each dataset is divided into five segments (using the original ordering of poses) representing the trajectories of five robots. Figure 14 shows the trajectories estimated by RBCD. Table 1 summarizes the quantitative results. On each dataset, we run RBCD with greedy selection for 1000 iterations, and compare the cost *after rounding* with the global minimum f_{MLE}^* obtained from the centralized solver [6]. In addition, we also report the final rotation RMSE ϵ_R and translation RMSE ϵ_t with respect to the centralized MLE solution, as well as the total amount of communication.

For comparison, we include the performance of DGN on all datasets after 1000 iterations. We observe that

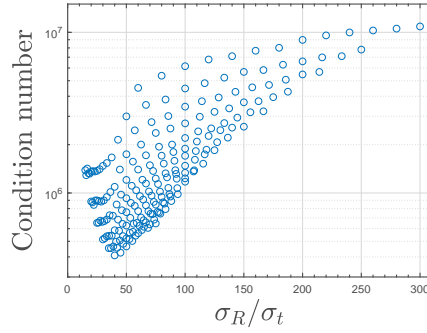


Figure 11: Average condition number of the connection Laplacian Q_T as a function of noise ratio σ_R/σ_t . To remove the trivial zero eigenvalue (see [6]), we anchor Q_T by removing a single row and column before calculating its condition number. Rotation noise varies from 3° to 15° . Translation noise varies from $0.05m$ to $0.2m$. For each pair (σ_R, σ_t) , 10 random noise realizations are generated and average condition number is recorded. As σ_R/σ_t increases, the conditioning of the problem becomes worse.

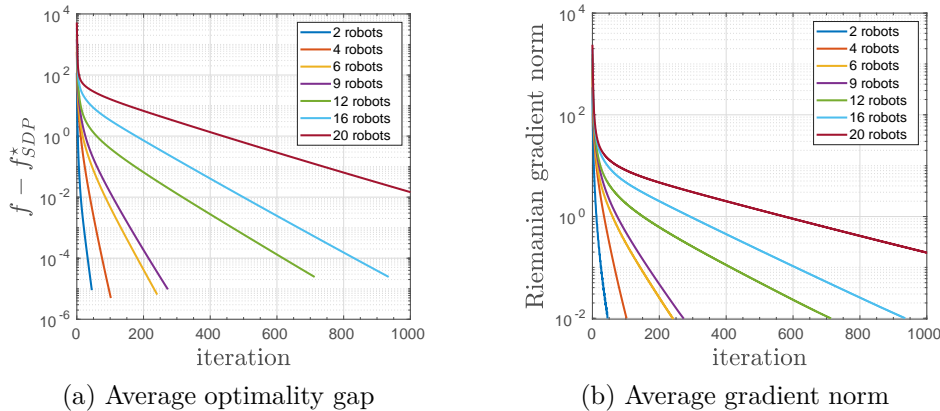


Figure 12: Convergence of RBCD with greedy block selection as the number of robots increases. Each robot owns 125 poses. $\sigma_R = 5^\circ, \sigma_t = 0.1m$. Results are averaged across 10 runs. (a) Average optimality gap $f - f_{SDP}^*$. (b) Average Riemannian gradient norm.

the convergence of DGN is very sensitive to the SOR relaxation parameter γ . In particular, the default value of $\gamma = 1$ does not produce the best convergence rate on most datasets. To ensure fair comparison, we run DGN with γ ranging from 0.1 to 1.9 and report the best result in Table 1. For reference, we also report the cost f_{DGN}^* after one centralized Gauss-Newton update, which serves as a lower bound on the final cost attained by DGN.

As shown in Table 1, RBCD produces near-optimal solutions on 6 out of 8 datasets (marked in green) when evaluated in terms of both cost and RMSE. A notable exception is KITTI 00, for which the returned solution has a clearly suboptimal cost and a nontrivial rotation RMSE. To explain this result, we note that the conditioning in KITTI 00 is particularly bad. After removing the trivial zero eigenvalue, the condition number of the connection Laplacian matrix is 1.24×10^{13} . In addition, on most datasets RBCD outperforms DGN. The difference in performance is clearer on 3D datasets compared to 2D datasets. We note that even with the best SOR relaxation parameter, DGN fails to converge on the parking garage and KITTI 00 datasets (marked in red). In contrast, the performance of RBCD is more stable since each iteration of RBCD is guaranteed to reduce the global cost function (Lemma 2). Finally, considering the large problem size, the communication induced by RBCD after 1000 iterations is fairly lightweight.

7.2 CNL Experiments

In this subsection, we evaluate RBCD on simulated CNL problems. During RBCD, instead of the default RTR update, we implement the optimal rotation and pose update rules as discussed in Section 4.3-4.4. Similar to

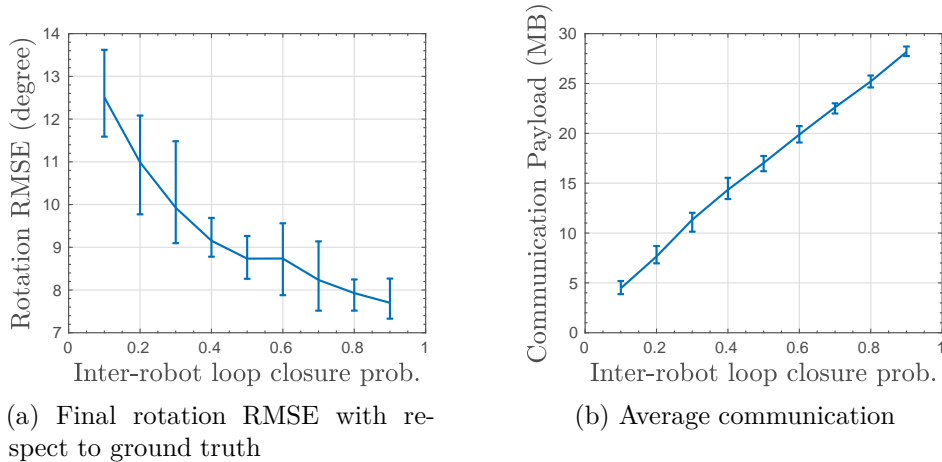


Figure 13: Performance of RBCD greedy after 1000 iterations as probability of inter-robot loop closure increases. We simulate 16 robots, each with 125 poses. Intra-robot loop closure is fixed at 0.1. Rotation noise is $\sigma_R = 5^\circ$ and translation noise is $\sigma_t = 0.1m$. Results are averaged across 10 runs. (a) Average rotation RMSE in degrees *with respect to the ground truth*, with the error bars denoting the range of RMSE across 10 runs. (b) Average communication costs in MB, with bars denoting the range of communication costs over 10 runs.

CSLAM, we compare the performance of RBCD against the baseline RGD algorithm. In addition, for rotation synchronization, we also compare against the generalized row-by-row (RBR) solver proposed in [7].

7.2.1 Convergence vs. RGD and RBR

Figure 15 shows convergence comparison for pose synchronization in the simulated 64 camera scenario (Figure 4a). Both RBCD and RGD are converging to the global minimum as suggested by the optimality gap and final RMSEs. Once again, RBCD with importance sampling and greedy selection demonstrate faster convergence compared to uniform sampling. Using the same simulations, we also test rotation synchronization and the results are shown in Figure 16. Interestingly, in this case RGD outperforms RBCD. Nevertheless, as shown in earlier experiments, RGD is not scalable to larger scale PGO instances (e.g., Figure 6 and Figure 7). In contrast, by taking advantage of the natural block-separable structures, RBCD is easily scalable to typical size CNL and CSLAM problems.

To further add to our experimental evaluations, we also compare RBCD against the RBR algorithm [7] for rotation synchronization. Since the per-iteration costs of the two algorithms are different, we evaluate performance as a function of runtime; see Figure 17. We have also included RGD for reference. In the 20 camera simulation (Figure 17a), RBCD significantly outperforms both RGD and RBR. In the 200 camera simulation (Figure 17b), RBCD is slower than RGD but still outperforms RBR. However, we note that this result largely reflects convergence rates in the centralized setting. In the distributed case, RGD will incur extra overhead due to the need to perform backtracking line search.

7.2.2 Varying Rank Relaxation

So far, we have focused on solving the rank-restricted SDPs under a fixed rank $r = 5$. In this section, we investigate the effect of varying r on the performance of local search algorithms. For this, we consider solving Problem 6 in a CNL simulation with 216 cameras and increased rotation noise $\sigma_R = 8^\circ$. As shown in Figure 18a-18b, with the default distributed chordal initialization, RBCD with greedy selection converges to global minimum under all values of r . In contrast, the rank relaxation plays a more important role when the initialization is bad. To illustrate this, Figure 18c-18d show results with random initialization. Under $r = 3$ and $r = 4$, RBCD converges to local minima. As we continue to relax the rank constraints (by increasing r), the algorithm is able to circumvent local minima and converge to the global solution. We note that even in the case

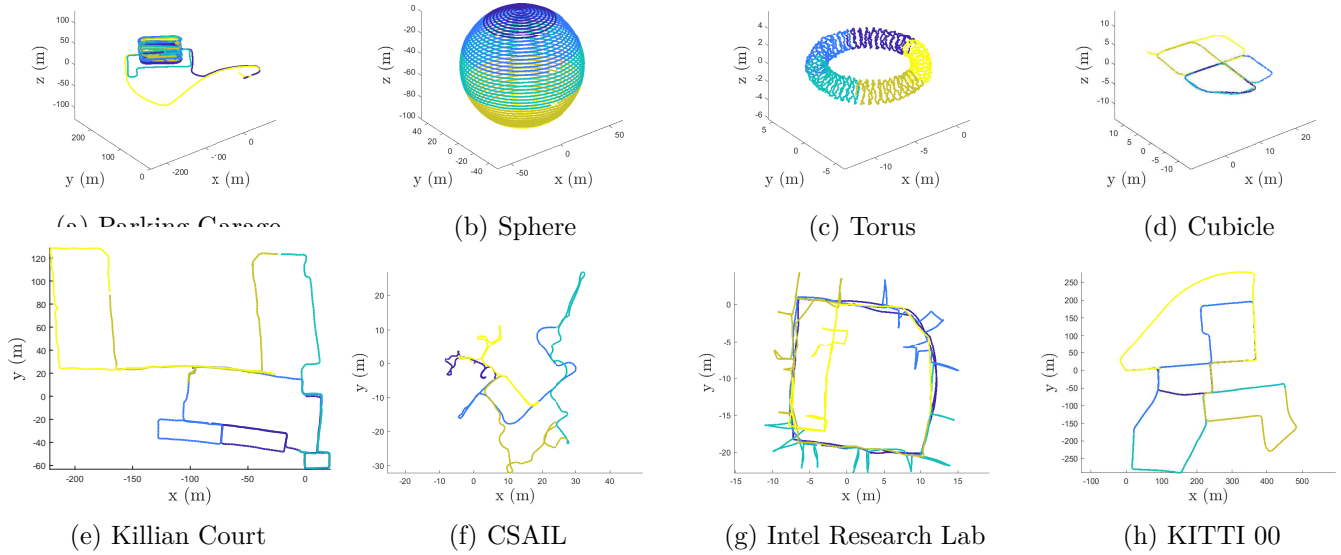


Figure 14: Solution returned by RBCD with greedy selection after 1000 iterations. Each color denotes the trajectory of a single robot. Datasets shown in the top row are in 3D, and those in the bottom row are in 2D.

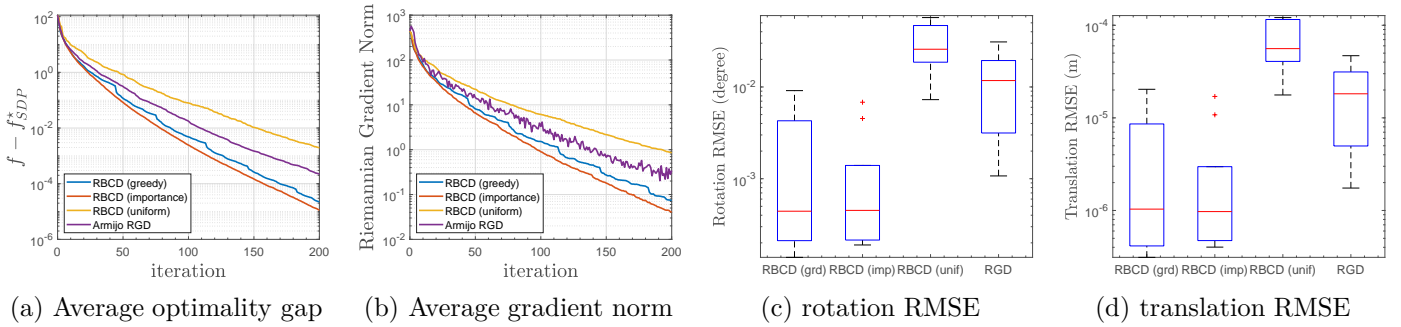


Figure 15: Pose synchronization results in the CNL scenario (Figure 4a). (a) Optimality gap $f - f_{SDP}^*$, (b) Riemannian gradient norm, (c) boxplot of final rotation RMSE, (d) boxplot of final translation RMSE. Results are averaged across 10 random instances.

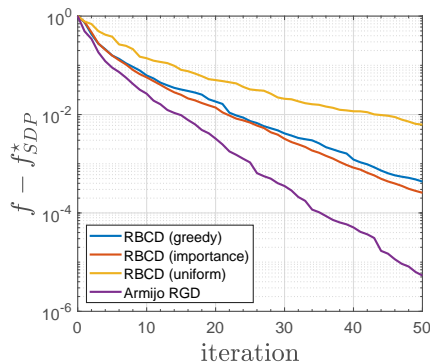
of small r (3 or 4), it is possible to recover from local minima via the escaping procedure after verification (see Section 6.2). Nevertheless, the results in this section suggests that in practice, with reasonable initialization, RBCD is not sensitive to the choice of r and typically converge to global minimizers at the first level of the Riemannian Staircase. Thus, in these more common scenarios, verification and escaping (Section 6.2) can be treated as an optional step.

8 Conclusion

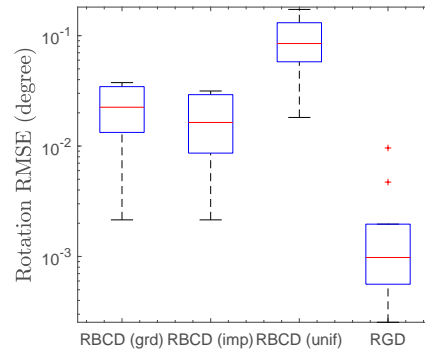
In this work, we presented a *certifiably correct* distributed PGO solver based on sparse SDP relaxations. By exploiting connections to state-of-the-art centralized SDP relaxation [5], we established formal performance guarantees for our SDP relaxation of pose synchronization in terms of the *existence of low-rank solutions* and *exactness under low noise*. To solve the resulting large-scale SDPs, we developed Riemannian block-coordinate descent (RBCD) as the core distributed procedure to solve rank-restricted surrogates of the SDP relaxations in the Riemannian Staircase framework. RBCD leverages the natural graphical structure of PGO to achieve computation and communication efficiency, privacy protection, and effective parallel implementation.

Table 1: Evaluation on benchmark SLAM datasets. Each dataset simulates a CSLAM scenario with five robots. f_{init} is the initial cost after distributed chordal initialization. f_{MLE}^* is the global minimum obtained from the centralized solver [6]. f_{DGN}^* is the cost after one centralized Gauss-Newton update. f_{DGN} is the cost after 1000 iterations of DGN [2] using the best SOR relaxation parameter. f_{RBCD} is the rounded cost of RBCD with greedy selection after 1000 iterations. ϵ_R and ϵ_t are the rotation and translation RMSE of the RBCD solution with respect to the centralized solution. Comm. is the total amount of communication in MB.

Datasets	# poses	# edges	f_{init}	f_{MLE}^* [6]	f_{DGN}^*	f_{DGN} [2]	f_{RBCD}	ϵ_R [deg]	ϵ_t [m]	Comm. [MB]
Parking Garage (3D)	1661	6275	4.477	1.263	1.268	2448	1.282	0.789	0.0111	23.31
Sphere (3D)	2500	4949	2058	1687	1687	1687	1687	2.52×10^{-4}	2.69×10^{-6}	4.71
Torus (3D)	5000	9048	24912	24227	24244	24244	24227	1.33×10^{-4}	1.13×10^{-7}	10.40
Cubicle (3D)	5750	16869	844	717.1	721.4	721.5	717.3	0.230	3.44×10^{-4}	33.96
Killian Court (2D)	808	827	263.7	61.15	66.76	66.76	63.66	5.6091	0.143	0.50
CSAIL (2D)	1045	1171	35.96	31.47	31.47	31.47	31.63	0.105	0.0035	1.42
Intel Research Lab (2D)	1228	1483	1201	393.7	393.7	393.7	393.7	1.39×10^{-3}	2.49×10^{-5}	1.70
KITTI 00 (2D)	4541	4676	2667	125.7	129.9	45986	242.4	2.05	0.054	3.70



(a) Average optimality gap



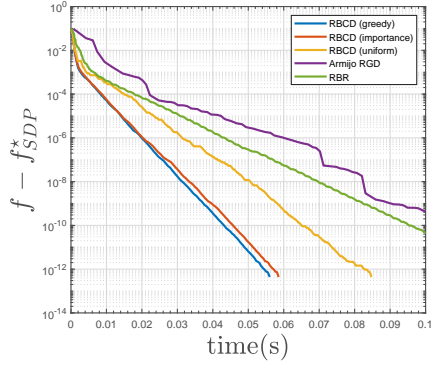
(b) rotation RMSE

Figure 16: Rotation synchronization results in the CNL scenario (Figure 4a). (a) Optimality gap $f - f_{\text{SDP}}^*$, (b) boxplot of final rotation RMSE. Results are averaged across 10 random instances.

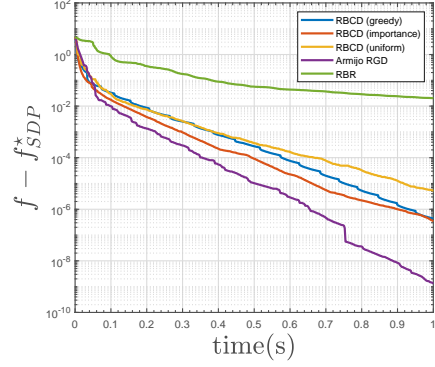
Furthermore, we proved that under mild conditions, RBCD converges to first-order critical points for general Riemannian optimization problems over product manifolds, with *global* sublinear convergence rate. Extensive evaluation showed that the proposed solver correctly identifies global solutions under low-to-moderate noise, and outperforms alternative distributed methods in terms of solution quality and convergence rate.

Acknowledgments

The authors would like to thank David Rosen and Luca Carlone for fruitful discussions that led to this work. This work was supported in part by the NASA Convergent Aeronautics Solutions project Design Environment for Novel Vertical Lift Vehicles (DELIVER), by ONR under BRC award N000141712072, and by ARL DCIST under Cooperative Agreement Number W911NF-17-2-0181.

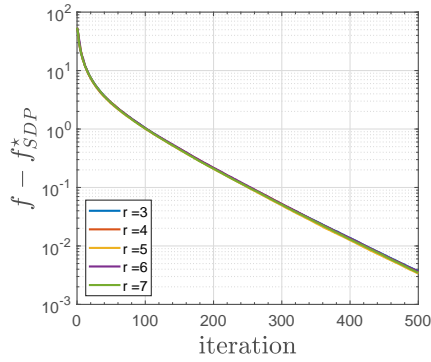


(a) 20 cameras

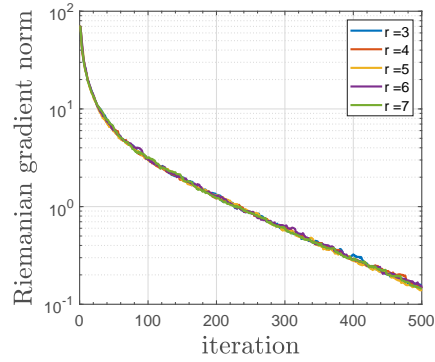


(b) 200 cameras

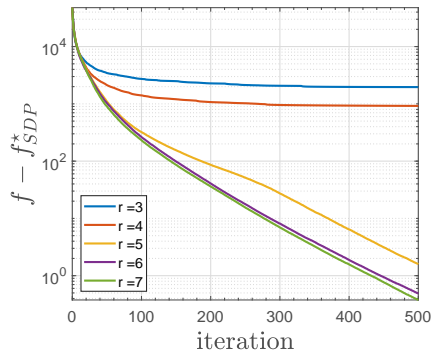
Figure 17: Optimality gap of RBCD, RGD, and RBR as a function of runtime. In the 20 camera simulation (a), RBCD significantly outperforms both RGD and RBR, and RBR outperforms RGD. In the 200 camera simulation (b), RBCD is slower compared to RGD, but still outperforms RBR.



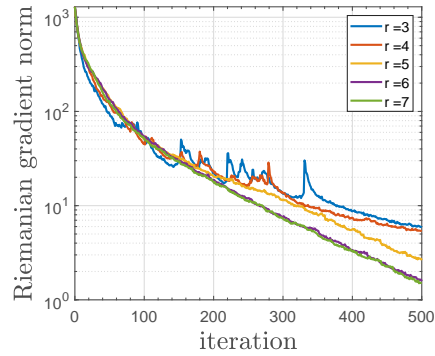
(a) Average optimality gap, dis-



(b) Average gradient norm, dis-



(c) Average optimality gap, random initialization



(d) Average gradient norm, random initialization

Figure 18: Convergence of RBCD on Problem 6 under different rank relaxations. The CNL simulation has 216 cameras, with rotation noise set to $\sigma_R = 8^\circ$. Results are averaged across 10 random runs. (a)-(b) show convergence with distributed chordal initialization, and (c)-(d) show convergence with random initialization.

References

- [1] P. Schmuck and M. Chli, “CCM-SLAM: Robust and efficient centralized collaborative monocular simultaneous localization and mapping for robotic teams,” *Journal of Field Robotics*, 2018.
- [2] S. Choudhary, L. Carlone, C. Nieto, J. Rogers, H. I. Christensen, and F. Dellaert, “Distributed mapping with privacy and communication constraints: Lightweight algorithms and object-based models,” *The International Journal of Robotics Research*, vol. 36, no. 12, pp. 1286–1311, 2017.
- [3] A. Cunningham, M. Paluri, and F. Dellaert, “DDF-SAM: Fully distributed SLAM using constrained factor graphs,” in *2010 IEEE/RSJ International Conference on Intelligent Robots and Systems*. IEEE, 2010, pp. 3025–3030.
- [4] A. Cunningham, V. Indelman, and F. Dellaert, “DDF-SAM 2.0: Consistent distributed smoothing and mapping,” in *2013 IEEE International Conference on Robotics and Automation*, May 2013, pp. 5220–5227.
- [5] D. M. Rosen, L. Carlone, A. S. Bandeira, and J. J. Leonard, “SE-Sync: A certifiably correct algorithm for synchronization over the special euclidean group,” *The International Journal of Robotics Research*, vol. 38, no. 2-3, pp. 95–125, 2019.
- [6] J. Briales and J. Gonzalez-Jimenez, “Cartan-Sync: Fast and global SE(d)-synchronization,” *IEEE Robotics and Automation Letters*, 2017.
- [7] A. Eriksson, C. Olsson, F. Kahl, and T.-J. Chin, “Rotation averaging with the chordal distance: Global minimizers and strong duality,” *IEEE transactions on pattern analysis and machine intelligence*, 2019.
- [8] T. Fan, H. Wang, M. Rubenstein, and T. Murphey, “Efficient and guaranteed planar pose graph optimization using the complex number representation,” in *2019 IEEE/RSJ International Conference on Intelligent Robots and Systems (IROS)*, 2019.
- [9] A. S. Bandeira, N. Boumal, and A. Singer, “Tightness of the maximum likelihood semidefinite relaxation for angular synchronization,” *Mathematical Programming*, vol. 163, no. 1, pp. 145–167, May 2017.
- [10] N. Boumal, “A Riemannian low-rank method for optimization over semidefinite matrices with block-diagonal constraints,” *arXiv preprint arXiv:1506.00575*, 2015.
- [11] S. Burer and R. D. C. Monteiro, “A nonlinear programming algorithm for solving semidefinite programs via low-rank factorization,” *Math. Program.*, vol. 95, pp. 329–357, 2003.
- [12] P.-A. Absil, C. G. Baker, and K. A. Gallivan, “Trust-region methods on riemannian manifolds,” *Foundations of Computational Mathematics*, vol. 7, no. 3, pp. 303–330, 2007.
- [13] P.-A. Absil, R. Mahony, and R. Sepulchre, *Optimization algorithms on matrix manifolds*. Princeton University Press, 2009.
- [14] K. Khosoussi, S. Huang, and G. Dissanayake, “A sparse separable SLAM back-end,” *IEEE Transactions on Robotics*, vol. 32, no. 6, pp. 1536–1549, 2016.
- [15] A. Singer, “Angular synchronization by eigenvectors and semidefinite programming,” *Applied and Computational Harmonic Analysis*, 2011.
- [16] R. Hartley, J. Trunpf, Y. Dai, and H. Li, “Rotation averaging,” *International Journal of Computer Vision*, 2013.
- [17] R. Tron, *Distributed optimization on manifolds for consensus algorithms and camera network localization*. The Johns Hopkins University, 2012.

- [18] R. Tron and R. Vidal, “Distributed 3-D localization of camera sensor networks from 2-D image measurements,” *IEEE Transactions on Automatic Control*, vol. 59, no. 12, pp. 3325–3340, Dec 2014.
- [19] R. Tron, J. Thomas, G. Loianno, K. Daniilidis, and V. Kumar, “A distributed optimization framework for localization and formation control: Applications to vision-based measurements,” *IEEE Control Systems Magazine*, vol. 36, no. 4, pp. 22–44, 2016.
- [20] T. Cieslewski, S. Choudhary, and D. Scaramuzza, “Data-efficient decentralized visual SLAM,” in *2018 IEEE International Conference on Robotics and Automation (ICRA)*. IEEE, 2018, pp. 2466–2473.
- [21] P.-Y. Lajoie, B. Ramtoula, Y. Chang, L. Carlone, and G. Beltrame, “DOOR-SLAM: Distributed, online, and outlier resilient SLAM for robotic teams,” *arXiv preprint arXiv:1909.12198*, 2019.
- [22] D. P. Bertsekas and J. N. Tsitsiklis, *Parallel and distributed computation: numerical methods*. Prentice hall Englewood Cliffs, NJ, 1989, vol. 23.
- [23] J. Nutini, I. Laradji, and M. Schmidt, “Let’s make block coordinate descent go fast: Faster greedy rules, message-passing, active-set complexity, and superlinear convergence,” 2017.
- [24] Y. Nesterov, “Efficiency of coordinate descent methods on huge-scale optimization problems,” *SIAM Journal on Optimization*, vol. 22, no. 2, pp. 341–362, 2012.
- [25] A. Beck and L. Tetruashvili, “On the convergence of block coordinate descent type methods,” *SIAM journal on Optimization*, vol. 23, no. 4, pp. 2037–2060, 2013.
- [26] T. Duckett, S. Marsland, and J. Shapiro, “Learning globally consistent maps by relaxation,” in *Robotics and Automation, 2000. Proceedings. ICRA ’00. IEEE International Conference on*, vol. 4. IEEE, 2000, pp. 3841–3846.
- [27] U. Frese, P. Larsson, and T. Duckett, “A multilevel relaxation algorithm for simultaneous localization and mapping,” *IEEE Transactions on Robotics*, vol. 21, no. 2, pp. 196–207, 2005.
- [28] R. Hartley, K. Aftab, and J. Trumpf, “L1 rotation averaging using the weiszfeld algorithm,” in *CVPR 2011*. IEEE, 2011, pp. 3041–3048.
- [29] A. Eriksson, C. Olsson, F. Kahl, and T.-J. Chin, “Rotation averaging and strong duality,” in *The IEEE Conference on Computer Vision and Pattern Recognition (CVPR)*, June 2018.
- [30] Z. Wen, D. Goldfarb, S. Ma, and K. Scheinberg, “Row by row methods for semidefinite programming,” *Industrial Engineering*, pp. 1–21, 2009.
- [31] P.-W. Wang, W.-C. Chang, and J. Z. Kolter, “The mixing method: low-rank coordinate descent for semidefinite programming with diagonal constraints,” *arXiv preprint arXiv:1706.00476*, 2017.
- [32] M. A. Erdogdu, A. Ozdaglar, P. A. Parrilo, and N. D. Vanli, “Convergence rate of block-coordinate maximization burer-monteiro method for solving large SDPs,” *arXiv preprint arXiv:1807.04428*, 2018.
- [33] Y. Tian, K. Khosoussi, and J. P. How, “Block-coordinate minimization for large SDPs with block-diagonal constraints,” *arXiv preprint arXiv:1903.00597*, 2019.
- [34] L. Carlone, R. Tron, K. Daniilidis, and F. Dellaert, “Initialization techniques for 3D SLAM: A survey on rotation estimation and its use in pose graph optimization,” in *2015 IEEE International Conference on Robotics and Automation (ICRA)*, May 2015, pp. 4597–4604.
- [35] L. Carlone, D. M. Rosen, G. Calafiore, J. J. Leonard, and F. Dellaert, “Lagrangian duality in 3D SLAM: Verification techniques and optimal solutions,” in *2015 IEEE/RSJ International Conference on Intelligent Robots and Systems (IROS)*, 2015, pp. 125–132.

- [36] A. I. Barvinok, “Problems of distance geometry and convex properties of quadratic maps,” *Discrete & Computational Geometry*, Mar 1995.
- [37] G. Pataki, “On the rank of extreme matrices in semidefinite programs and the multiplicity of optimal eigenvalues,” *Mathematics of Operations Research*, 05 1998.
- [38] N. Boumal, V. Voroninski, and A. S. Bandeira, “The non-convex burer–monteiro approach works on smooth semidefinite programs,” in *Proceedings of the 30th International Conference on Neural Information Processing Systems*. USA: Curran Associates Inc., 2016, pp. 2765–2773.
- [39] A. Javanmard, A. Montanari, and F. Ricci-Tersenghi, “Phase transitions in semidefinite relaxations.” *Proceedings of the National Academy of Sciences (PNAS)*, 2016.
- [40] D. Rosen and L. Carlone, “Computational enhancements for certifiably correct SLAM,” 2017, workshop on “Introspective Methods for Reliable Autonomy”.
- [41] R. Lai and S. Osher, “A splitting method for orthogonality constrained problems,” *Journal of Scientific Computing*, 2014.
- [42] L. Barenboim and M. Elkin, “Distributed $(\delta+1)$ -coloring in linear (in δ) time,” in *Proceedings of the forty-first annual ACM symposium on Theory of computing*. ACM, 2009, pp. 111–120.
- [43] J. Schneider and R. Wattenhofer, “A new technique for distributed symmetry breaking,” in *Proceedings of the 29th ACM SIGACT-SIGOPS symposium on Principles of distributed computing*. ACM, 2010, pp. 257–266.
- [44] N. Boumal, P.-A. Absil, and C. Cartis, “Global rates of convergence for nonconvex optimization on manifolds,” *IMA Journal of Numerical Analysis*, vol. 39, no. 1, pp. 1–33, 02 2018.
- [45] S. Leonardos, V. Preciado, and K. Daniilidis, “A dynamical systems approach to distributed eigenvector computation,” in *2017 IEEE 56th Annual Conference on Decision and Control (CDC)*, Dec 2017, pp. 2209–2215.
- [46] N. Boumal, B. Mishra, P.-A. Absil, and R. Sepulchre, “Manopt, a Matlab toolbox for optimization on manifolds,” *Journal of Machine Learning Research*, 2014. [Online]. Available: <http://www.manopt.org>
- [47] R. A. Horn and C. R. Johnson, *Topics in Matrix Analysis*. Cambridge University Press, 1991.

Table 2: A list of problems considered in this work. Shaded rows correspond to the pose synchronization problem, while other rows correspond to the rotation synchronization problem. Here $i \in [n]$ where n is the number of nodes in the problem. The dimension of the problem is denoted by $d \in \{2, 3\}$. We note that Problem 5 and 8 are not directly used in the proposed approach, but are nonetheless crucial for establishing the performance guarantees of the SDP relaxation for pose synchronization (Theorem 1 and Theorem 2).

#	Problem Description	Cost Function	Domain	Constraints
1	MLE for Rotation Sync	(8a)	$R_i \in \text{SO}(d)$	–
2	MLE for Pose Sync	(10a)	$(R_i, t_i) \in \text{SO}(d) \times \mathbb{R}^d$	–
3	SDP Relaxation of Rotation Sync	$\text{tr}(Q_R Z_R)$	$Z_R \in \mathbb{S}_{\geq 0}^{dn}$	$Z_{R[i,i]} = I_d$
4	Full SDP Relaxation of Pose Sync	$\text{tr}(Q_T Z_T)$	$Z_T \in \mathbb{S}_{\geq 0}^{n+dn}$	$Z_{T[i,i](1:d,1:d)} = I_d$
5	Rotation-only SDP Relaxation for Pose Sync	$\text{tr}(\tilde{Q}_T Z_R)$	$Z_R \in \mathbb{S}_{\geq 0}^{dn}$	$Z_{R[i,i]} = I_d$
6	Rank-Restricted SDP for Rotation Sync	$\text{tr}(Q_R Y^\top Y)$	$Y \in \text{St}(d, r)^n$	–
7	Rank-Restricted Full SDP for Pose Sync	$\text{tr}(Q_T X^\top X)$	$X \in (\text{St}(d, r) \times \mathbb{R}^r)^n$	–
8	Rotation-only Rank-Restricted SDP for Pose Sync	$\text{tr}(\tilde{Q}_T Y^\top Y)$	$Y \in \text{St}(d, r)^n$	–

Appendices

A Proof of Theorem 1

We begin by giving the formal definition of the cost matrix that appears in the rotation-only SDP relaxation (Problem 5); see also [5, Equation 20(b)],

$$\tilde{Q}_T \triangleq Q_R + \tilde{\Sigma} - \tilde{V}^\top L(W^\tau)^\dagger \tilde{V}, \quad (50)$$

In (50), $Q_R \in \mathbb{S}_{\geq 0}^{dn}$ is the rotation connection Laplacian (same as the cost matrix in Problem 3), and $L(W^\tau) \in \mathbb{S}_{\geq 0}^n$ is the graph Laplacian of the pose graph with edges weighted by the translation measurement weights $\{\tau_{ij}\}$. The remaining two matrices $\tilde{V} \in \mathbb{R}^{n \times dn}$ and $\tilde{\Sigma} \in \mathbb{R}^{dn \times dn}$ are formed using translation measurements and are defined in equations (15) and (16) in [5], respectively. In this section, we also consider the rank-restricted version of Problem 5, defined below (see also [5, Problem 9]).

Problem 8 (Rotation-only Rank-restricted SDP for Pose Synchronization [5]).

$$\underset{Y \in \text{St}(d, r)^n}{\text{minimize}} \quad \text{tr}(\tilde{Q}_T Y^\top Y). \quad (51)$$

The rank-restricted SDP solved in this work (Problem 7) and the rotation-only rank-restricted SDP defined above (Problem 8) are tightly connected. The following lemma precisely characterizes this connection.

Lemma 3. For a given $X^* = [Y_1^* \ p_1^* \ \dots \ Y_n^* \ p_n^*] \in (\text{St}(d, r) \times \mathbb{R}^r)^n$, define $Y^* \triangleq [Y_1^* \ \dots \ Y_n^*] \in \text{St}(d, r)^n$ and $p^* \triangleq [p_1^* \ \dots \ p_n^*] \in \mathbb{R}^{r \times n}$. Then, X^* is optimal to Problem 7 if and only if Y^* is optimal to Problem 8 and $p^* = -Y^* \tilde{V}^\top L(W^\tau)^\dagger + c \mathbf{1}_n^\top$, for some $c \in \mathbb{R}^r$. Furthermore, $\text{tr}(Q_T X^{*\top} X^*) = \text{tr}(\tilde{Q}_T Y^{*\top} Y^*)$.

Proof. We show that Problem 8 can be obtained from Problem 7 by analytically eliminating the Euclidean variables. A detailed derivation of this result is already presented in [5, Appendix B] for $r = d$. For $r \geq d$, the

proof is largely identical with minor modifications to the dimensions of certain matrices. For this reason, we only give a sketch of the proof and refer the readers to [5, Appendix B] for the complete technical details.

Let $X = \begin{bmatrix} Y_1 & p_1 & \dots & Y_n & p_n \end{bmatrix} \in (\text{St}(d, r) \times \mathbb{R}^r)^n$ be the decision variable in Problem 7. Let $Y = \begin{bmatrix} Y_1 & \dots & Y_n \end{bmatrix} \in \text{St}(d, r)^n$ and $p = \begin{bmatrix} p_1 & \dots & p_n \end{bmatrix} \in \mathbb{R}^{r \times n}$. From the definition of the connection Laplacian Q_T (see [6, Appendix II]), it can be shown that the cost function in Problem 7 can be expanded into the following,

$$\text{tr}(Q_T X^\top X) = \sum_{(i,j) \in \mathcal{E}} \kappa_{ij} \|Y_j - Y_i \tilde{R}_{ij}\|_F^2 + \sum_{(i,j) \in \mathcal{E}} \tau_{ij} \|p_j - p_i - Y_i \tilde{t}_{ij}\|_2^2. \quad (52)$$

Since (52) is an unconstrained convex quadratic problem over $\{p_i\}_{i=1}^n$, we can analytically eliminate these variables from Problem 7 by substituting in their closed-form solutions (as a function of Y) using the generalized Schur complement. To do this in a compact form, starting from (52), vectorize Problem 7 into the following quadratic problem with non-convex constraints,

$$\underset{Y \in \text{St}(d, r)^n, p \in \mathbb{R}^{r \times n}}{\text{minimize}} \begin{bmatrix} \text{vec}(p) \\ \text{vec}(Y) \end{bmatrix}^\top (M \otimes I_r) \begin{bmatrix} \text{vec}(p) \\ \text{vec}(Y) \end{bmatrix}, \quad (53)$$

$$M \triangleq \begin{bmatrix} L(W^\tau) & \tilde{V} \\ \tilde{V}^\top & Q_R + \tilde{\Sigma} \end{bmatrix}. \quad (54)$$

In (53), the $\text{vec}(\cdot)$ operator concatenates columns of the input matrix into a single vector. The full derivation from (52) to (53) is presented in [5, Appendix B.1]. We note that the only difference in our case is that d is now replaced by r .

The rest of the proof follows [5, Appendix B.2]. Define $A \triangleq L(W^\tau) \otimes I_r$ and $b \triangleq (\tilde{V} \otimes I_r) \text{vec}(Y)$. By the definition of graph Laplacian and [47, Theorem 4.2.12], A is necessarily positive semidefinite. Furthermore, $\text{rank}(A) = rn - r$ and the kernel of A is spanned by the columns of $U \triangleq \mathbf{1}_n \otimes I_r$. We can equivalently express $\ker(A)$ as (cf. [5, Equation (76)]),

$$\ker(A) = \{Uc \mid c \in \mathbb{R}^r\} = \{\text{vec}(c \mathbf{1}_n^\top) \mid c \in \mathbb{R}^r\}. \quad (55)$$

Next, we show that $b \perp \ker(A)$. From $\text{vec}(ABC) = (C^\top \otimes A) \text{vec}(B)$ (see [47, Lemma 4.3.1]), it holds that $b = \text{vec}(Y \tilde{V}^\top)$. Consider any null vector $u = \text{vec}(c \mathbf{1}_n^\top) \in \ker(A)$ where $c \in \mathbb{R}^r$. One can show that b is orthogonal to u ,

$$\langle b, u \rangle = \langle Y \tilde{V}^\top, c \mathbf{1}_n^\top \rangle = \text{tr}(\mathbf{1}_n^\top \tilde{V} Y^\top c) = 0. \quad (56)$$

This is because $\mathbf{1}_n^\top \tilde{V} = 0$ by the definition of \tilde{V} ; see Equation (15) in [5]. Since $A \succeq 0$ and $b \perp \ker(A)$, we can apply [5, Lemma 4] which gives the closed-form solution of p given Y . Specifically, the family of optimal p^* (as a function of Y) in vector form is characterized by,

$$\text{vec}(p^*(Y)) \in \{ - [L(W^\tau) \otimes I_r]^\dagger (\tilde{V} \otimes I_r) \text{vec}(Y) + Uc \mid c \in \mathbb{R}^r \}. \quad (57)$$

Using [47, Lemma 4.3.1], we can convert (57) back to matrix form (cf. [5, Equation (21)]),

$$p^*(Y) \in \{ - Y \tilde{V}^\top L(W^\tau)^\dagger + c \mathbf{1}_n^\top \mid c \in \mathbb{R}^r \}. \quad (58)$$

Finally, plugging (57) into (53) produces the following rotation-only problem (in vectorized form),

$$\underset{Y \in \text{St}(d, r)^n}{\text{minimize}} \text{vec}(Y)^\top [(Q_R + \tilde{\Sigma} - \tilde{V}^\top L(W^\tau)^\dagger \tilde{V}) \otimes I_r] \text{vec}(Y) = \text{vec}(Y)^\top [\tilde{Q}_T \otimes I_r] \text{vec}(Y) \quad (59)$$

In matrix form, the above problem can be written as,

$$\underset{Y \in \text{St}(d, r)^n}{\text{minimize}} \text{tr}(\tilde{Q}_T Y^\top Y), \quad (60)$$

which is exactly Problem 8. This shows that after analytically eliminating p , Problem 7 and Problem 8 are equivalent, which concludes the proof. \square

With Lemma 3, we are now ready to give the proof of Theorem 1.

Proof of Theorem 1. We give a constructive proof where we show that from a minimizer $Z_{\text{T}}^* \in \mathbb{S}_{\geq 0}^{n+dn}$ to Problem 4, we can recover a minimizer $Z_{\text{R}}^* \in \mathbb{S}_{\geq 0}^{dn}$ to Problem 5 with the same rank, and vice versa.

(\Rightarrow) Let $Z_{\text{T}}^* \in \mathbb{S}_{\geq 0}^{n+dn}$ be a minimizer to Problem 4 with $\text{rank}(Z_{\text{T}}^*) = r$. Consider the rank- r factorization $Z_{\text{T}}^* = X^{*\top} X^*$, where $X^* = \begin{bmatrix} Y_1^* & p_1^* & \dots & Y_n^* & p_n^* \end{bmatrix} \in (\text{St}(d, r) \times \mathbb{R}^r)^n$. Define $Y^* \triangleq \begin{bmatrix} Y_1^* & \dots & Y_n^* \end{bmatrix} \in \text{St}(d, r)^n$ and $Z_{\text{R}}^* \triangleq Y^{*\top} Y^*$. We now show that Z_{R}^* is a minimizer to Problem 5. First, we note that X^* is an optimal solution to the rank-restricted SDP (Problem 7) with rank r . By Lemma 3 it thus holds that,

$$\text{tr}(Q_{\text{T}} Z_{\text{T}}^*) = \text{tr}(Q_{\text{T}} X^{*\top} X^*) \quad (Z_{\text{T}}^* = X^{*\top} X^*) \quad (61)$$

$$= \text{tr}(\tilde{Q}_{\text{T}} Y^{*\top} Y^*) \quad (\text{by Lemma 3}) \quad (62)$$

$$= \text{tr}(\tilde{Q}_{\text{T}} Z_{\text{R}}^*). \quad (Z_{\text{R}}^* \triangleq Y^{*\top} Y^*) \quad (63)$$

Suppose for the sake of contradiction that Z_{R}^* is not a solution to Problem 5. Then, there exists a feasible $Z_{\text{R}}^\diamond \in \mathbb{S}_{\geq 0}^{dn}$ such that $\text{tr}(\tilde{Q}_{\text{T}} Z_{\text{R}}^\diamond) < \text{tr}(\tilde{Q}_{\text{T}} Z_{\text{R}}^*)$. Let $\text{rank}(Z_{\text{R}}^\diamond) = r'$, and consider the rank- r' factorization $Z_{\text{R}}^\diamond = Y^{\diamond\top} Y^\diamond$ where $Y^\diamond \in \text{St}(d, r')^n$. Note that Y^\diamond is also a minimizer to Problem 8 with rank r' . Let $X^\diamond = \begin{bmatrix} Y_1^\diamond & p_1^\diamond & \dots & Y_n^\diamond & p_n^\diamond \end{bmatrix} \in (\text{St}(d, r) \times \mathbb{R}^{r'})^n$ be a corresponding minimizer to Problem 7 where the Euclidean components $p^\diamond = \begin{bmatrix} p_1^\diamond & \dots & p_n^\diamond \end{bmatrix}$ are recovered using (58). Define $Z_{\text{T}}^\diamond \triangleq X^{\diamond\top} X^\diamond$. By Lemma 3,

$$\text{tr}(Q_{\text{T}} Z_{\text{T}}^\diamond) = \text{tr}(Q_{\text{T}} X^{\diamond\top} X^\diamond) \quad (Z_{\text{T}}^\diamond \triangleq X^{\diamond\top} X^\diamond) \quad (64)$$

$$= \text{tr}(\tilde{Q}_{\text{T}} Y^{\diamond\top} Y^\diamond) \quad (\text{by Lemma 3}) \quad (65)$$

$$= \text{tr}(\tilde{Q}_{\text{T}} Z_{\text{R}}^\diamond). \quad (Z_{\text{R}}^\diamond = Y^{\diamond\top} Y^\diamond) \quad (66)$$

Combining (63), (66) and $\text{tr}(\tilde{Q}_{\text{T}} Z_{\text{R}}^\diamond) < \text{tr}(\tilde{Q}_{\text{T}} Z_{\text{R}}^*)$ we obtain,

$$\text{tr}(Q_{\text{T}} Z_{\text{T}}^\diamond) < \text{tr}(Q_{\text{T}} Z_{\text{T}}^*), \quad (67)$$

which contradicts our assumption that Z_{T}^* is a minimizer to Problem 4. Thus, Z_{R}^* must also be a minimizer to Problem 5.

(\Leftarrow) Let $Z_{\text{R}}^* \in \mathbb{S}_{\geq 0}^{dn}$ be a minimizer to Problem 5 with $\text{rank}(Z_{\text{R}}^*) = r$. Consider a rank- r factorization $Z_{\text{R}}^* = Y^{*\top} Y^*$ where $Y^* = \begin{bmatrix} Y_1^* & \dots & Y_n^* \end{bmatrix} \in \text{St}(d, r)^n$. Once again, Y^* must be a minimizer to Problem 8 with rank r . Let $X^* = \begin{bmatrix} Y_1^* & p_1^* & \dots & Y_n^* & p_n^* \end{bmatrix} \in (\text{St}(d, r) \times \mathbb{R}^r)^n$ be a corresponding minimizer to Problem 7 where the Euclidean components $p^* = \begin{bmatrix} p_1^* & \dots & p_n^* \end{bmatrix}$ are recovered using (58). Define $Z_{\text{T}}^* \triangleq X^{*\top} X^*$. Using the same proof by contradiction technique as in (\Rightarrow), we can show that Z_{T}^* must be a minimizer to Problem 4.

To conclude the proof, note that in both (\Rightarrow) and (\Leftarrow), we have $\text{rank}(Z_{\text{T}}^*) = \text{rank}(Z_{\text{R}}^*)$ by construction. Furthermore, (63) suggests that $\text{tr}(Q_{\text{T}} Z_{\text{T}}^*) = \text{tr}(\tilde{Q}_{\text{T}} Z_{\text{R}}^*)$. Since Z_{T}^* and Z_{R}^* are minimizers of Problems 4 and 5, respectively, this equality must also hold for *all* minimizers of these two problems. \square

B Proof of Theorem 2

We now state the formal version of Theorem 2, which is first presented informally in Section 3.2.

Theorem 2 (Exact recovery via Problem 4). Let \underline{Q} be the matrix of the form (50) constructed using the ground truth relative transforms $(\underline{R}_{ij}, \underline{t}_{ij})$. There exists a constant $\beta \triangleq \beta(\underline{Q})$ such that if $\|\tilde{Q}_{\text{T}} - \underline{Q}\|_2 < \beta$, every minimizer Z_{T}^* to Problem 4 has its first $d \times (n + dn)$ block row given by $Z_{\text{T}(1:d,:)}^* = \begin{bmatrix} R_1^* & t_1^* & \dots & R_n^* & t_n^* \end{bmatrix}$, where $\{R_i^*, t_i^*\}$ is an optimal solution to Problem 2.

Proof. By [5, Proposition 2], there exists a constant $\beta \triangleq \beta(Q)$ such that if $\|\tilde{Q}_T - Q\|_2 < \beta$, the rotation-only SDP relaxation (Problem 5) has a *unique* solution $Z_R^\circ = R^{\circ\top} R^\circ$, where $R^\circ = [R_1^\circ \ \dots \ R_n^\circ] \in \text{SO}(d)^n$ is the rotation component of an optimal solution to Problem 2. Let $T^\circ = [R_1^\circ \ t_1^\circ \ \dots \ R_n^\circ \ t_n^\circ] \in (\text{SO}(d) \times \mathbb{R}^d)^n$ be a corresponding full minimizer to Problem 2, where the optimal translations are recovered by using (58) with $c = 0$,

$$t^\circ = [t_1^\circ \ \dots \ t_n^\circ] = -R^\circ \tilde{V}^\top L(W^\tau)^\dagger. \quad (68)$$

Consider an optimal solution Z_T^\star to Problem 4. Since $Z_T^\star \succeq 0$, there always exists a factorization $Z_T^\star = X^{\star\top} X^\star$ for some $X^\star = [Y_1^\star \ p_1^\star \ \dots \ Y_n^\star \ p_n^\star] \in (\text{St}(d, r) \times \mathbb{R}^r)^n$ where $r \geq d$.⁸ Define $Y^\star \triangleq [Y_1^\star \ \dots \ Y_n^\star] \in \text{St}(d, r)^n$ and $p^\star = [p_1^\star \ \dots \ p_n^\star] \in \mathbb{R}^{r \times n}$. Note that since $X^{\star\top} X^\star$ is a minimizer to Problem 4, X^\star must be a minimizer to Problem 7 with rank r . Therefore, by Lemma 3,

$$\text{tr}(Q_T X^{\star\top} X^\star) = \text{tr}(\tilde{Q}_T Y^{\star\top} Y^\star). \quad (69)$$

Furthermore, by Theorem 1, it holds that,

$$\text{tr}(Q_T Z_T^\star) = \text{tr}(\tilde{Q}_T Z_R^\circ). \quad (70)$$

Therefore, we have,

$$\text{tr}(Q_T Z_T^\star) = \text{tr}(Q_T X^{\star\top} X^\star) \quad (Z_T^\star = X^{\star\top} X^\star) \quad (71)$$

$$= \text{tr}(\tilde{Q}_T Y^{\star\top} Y^\star) \quad (\text{Lemma 3}) \quad (72)$$

$$= \text{tr}(\tilde{Q}_T Z_R^\circ) \quad (70) \quad (73)$$

$$= \text{tr}(\tilde{Q}_T R^{\circ\top} R^\circ). \quad (Z_R^\circ = R^{\circ\top} R^\circ) \quad (74)$$

By [5, Proposition 2], it must hold that $Y^{\star\top} Y^\star = R^{\circ\top} R^\circ$ is the unique minimizer to Problem 5. Note that this immediately implies $\text{rank}(Y^\star) = \text{rank}(R^\circ) = d$. Consider the (thin) rank- d singular value decomposition $Y^\star = U_d \Sigma_d V_d^\top$, and define $\bar{Y} \triangleq \Sigma_d V_d^\top$. Since $U_d \in \text{St}(d, r)$, it must hold that $\bar{Y}^\top \bar{Y} = R^{\circ\top} R^\circ$, and hence $\bar{Y} \in \text{O}(d)^n$. Inspecting the first block row of this equality shows that, for all $i \in [n]$,

$$\bar{Y}_1^\top \bar{Y}_i = R_1^{\circ\top} R_i^\circ. \quad (75)$$

Multiplying both sides in (75) from the left by $U_d \bar{Y}_1$ shows that, for all $i \in [n]$,

$$Y_i^\star = U_d \bar{Y}_1 R_1^{\circ\top} R_i^\circ. \quad (76)$$

Let $A \triangleq U_d \bar{Y}_1 R_1^{\circ\top}$. We therefore have,

$$Y^\star = A R^\circ. \quad (77)$$

Since $U_d \in \text{St}(d, r)$ and $\bar{Y}_1, R_1^\circ \in \text{O}(d)$, we have $A \in \text{St}(d, r)$. See [5, Equations (45)-(49)] for similar derivations. By (77) and Lemma 3, there exists a $c \in \mathbb{R}^r$ such that,

$$p^\star = -Y^\star \tilde{V}^\top L(W^\tau)^\dagger + c \mathbf{1}_n^\top \quad (\text{Lemma 3}) \quad (78)$$

$$= -A R^\circ \tilde{V}^\top L(W^\tau)^\dagger + c \mathbf{1}_n^\top \quad (77) \quad (79)$$

$$= A t^\circ + c \mathbf{1}_n^\top. \quad (\text{Definition of } t^\circ) \quad (80)$$

Using (77) and (80), we can rewrite X^\star as,

$$X^\star = \left[\underbrace{A R_1^\circ}_{Y_1^\star} \quad \underbrace{A t_1^\circ + c}_{p_1^\star} \quad \dots \quad \underbrace{A R_n^\circ}_{Y_n^\star} \quad \underbrace{A t_n^\circ + c}_{p_n^\star} \right]. \quad (81)$$

⁸It is necessarily true that $r \geq \text{rank}(Z_T^\star) \geq d$, since the first d columns of Z_T^\star are constrained to be linearly independent.

To conclude the proof, we note that the first $d \times (n + dn)$ block row of $Z_T^* = X^{*\top} X^*$ is given by,

$$Z_{T(1:d,:)}^* = (AR_1^\circ)^\top \begin{bmatrix} AR_1^\circ & At_1^\circ + c & \dots & AR_n^\circ & At_n^\circ + c \end{bmatrix} \quad (82)$$

$$= \begin{bmatrix} \underbrace{I_d}_{R_1^*} & \underbrace{R_1^{\circ\top} t_1^\circ + R_1^{\circ\top} A^\top c}_{t_1^*} & \dots & \underbrace{R_1^{\circ\top} R_n^\circ}_{R_n^*} & \underbrace{R_1^{\circ\top} t_n^\circ + R_1^{\circ\top} A^\top c}_{t_1^*} \end{bmatrix}. \quad (83)$$

In particular, for all $i \in [n]$,

$$R_i^* = R_1^{\circ\top} R_i^\circ, \quad (84)$$

$$t_i^* = R_1^{\circ\top} t_i^\circ + R_1^{\circ\top} A^\top c. \quad (85)$$

In other words, $Z_{T(1:d,:)}^*$ can be obtained from T° via a global rigid body transformation with rotation $R_1^{\circ\top}$ and translation $R_1^{\circ\top} A^\top c$. Since T° is an optimal solution to Problem 2, $Z_{T(1:d,:)}^*$ is also an optimal solution due to the global gauge symmetry. \square

We conclude this section with an additional remark on Theorem 2. From (84), it can be seen that the first rotation is actually the identity matrix, i.e., $R_1^* = I_d$. We note that this is caused by our choice to look at the first block row of Z_T^* . In general, the same result in Theorem 2 extends trivially to other block rows of Z_T^* . In the paper, we have omitted this trivial extension for brevity.

C Proof of Corollary 1

Proof. Since the rotation-only SDP relaxation (Problem 5) has a compact search space, applying the theorem of Pataki [37] guarantees the existence of a low-rank solution Z_R^* with $\text{rank}(Z_R^*) \leq (d+1)\sqrt{n}$ (cf. [10, Equation (3)]). Applying Theorem 1 directly shows that Problem 4 must admit a minimizer Z_T^* with the same rank. \square

D Proof of Lemma 1

In [44], Boumal et al. establish a simple condition under which a function $f : \mathcal{M} \rightarrow \mathbb{R}$ has Lipschitz-type gradient for its pullbacks. For convenience, we include their result below:

Lemma 4 (Lemma 2.7 in [44]). Let \mathcal{E} be a Euclidean space and let \mathcal{M} be a compact Riemannian submanifold of \mathcal{E} . Let Retr be a retraction on \mathcal{M} (globally defined). If $f : \mathcal{E} \rightarrow \mathbb{R}$ has Lipschitz continuous gradient then the pullbacks $f \circ \text{Retr}_x$ satisfy (34) globally with some constant c_g independent of x .

In this work, we use an extension of Lemma 4 which we prove next.

Lemma 5 (Extension of Lemma 4 to product manifolds with Euclidean spaces). Let \mathcal{E}_1 and \mathcal{E}_2 be Euclidean spaces, and define $\mathcal{E} \triangleq \mathcal{E}_1 \times \mathcal{E}_2$. Let $\mathcal{M} \triangleq \mathcal{M}_1 \times \mathcal{E}_2$, where \mathcal{M}_1 is a compact Riemannian submanifold of \mathcal{E}_1 . Given $x = \begin{bmatrix} x_1 & x_2 \end{bmatrix} \in \mathcal{M}$ and $\eta = \begin{bmatrix} \eta_1 & \eta_2 \end{bmatrix} \in T_x \mathcal{M}$, define a retraction operator $\text{Retr}_x : T_x \mathcal{M} \rightarrow \mathcal{M}$ as: $\text{Retr}_x(\eta) = \begin{bmatrix} \text{Retr}_{x_1}(\eta_1) & \text{Retr}_{x_2}(\eta_2) \end{bmatrix} = \begin{bmatrix} \text{Retr}_{x_1}(\eta_1) & x_2 + \eta_2 \end{bmatrix}$, where Retr_{x_1} is a globally defined retraction on \mathcal{M}_1 and we employ the standard retraction for Euclidean space. If $f : \mathcal{E} \rightarrow \mathbb{R}$ has Lipschitz continuous gradient, then the pullbacks $f \circ \text{Retr}_x$ satisfy (34) globally with some constant c_g independent of x ; i.e.,

$$|\hat{f}_x(\eta) - [f(x) + \langle \eta, \text{grad}_x f \rangle]| \leq \frac{c_g}{2} \|\eta\|_2^2. \quad (86)$$

Proof. This proof is a straightforward generalization of the proof of Lemma 4. By assumption, the Euclidean gradient ∇f is Lipschitz continuous, i.e., there exists $L \geq 0$ such that for any $x, y \in \mathcal{M}$,

$$|f(y) - [f(x) + \langle \nabla_x f, y - x \rangle]| \leq \frac{L}{2} \|y - x\|^2. \quad (87)$$

The above equality is true in particular for any $y = \text{Retr}_x(\eta), \eta \in T_x \mathcal{M}$. In this case, the inner product that appears in the LHS of (87) can be expanded as,

$$\langle \nabla_x f, \text{Retr}_x(\eta) - x \rangle = \langle [\nabla_{x_1} f \quad \nabla_{x_2} f], [\text{Retr}_{x_1}(\eta_1) - x_1 \quad (x_2 + \eta_2) - x_2] \rangle \quad (88)$$

$$= \langle \nabla_{x_1} f, \text{Retr}_{x_1}(\eta_1) - x_1 \rangle + \langle \nabla_{x_2} f, \eta_2 \rangle \quad (89)$$

$$= \langle \nabla_{x_1} f, \text{Retr}_{x_1}(\eta_1) - x_1 - \eta_1 + \eta_1 \rangle + \langle \nabla_{x_2} f, \eta_2 \rangle \quad (\text{Add and subtract } \eta_1) \quad (90)$$

$$= \langle \nabla_{x_1} f, \eta_1 \rangle + \langle \nabla_{x_2} f, \eta_2 \rangle + \langle \nabla_{x_1} f, \text{Retr}_{x_1}(\eta_1) - x_1 - \eta_1 \rangle. \quad (91)$$

Next, we use two facts (1) Riemannian gradient in Euclidean spaces equals Euclidean gradient; and (2) Riemannian gradient for general manifolds is the orthogonal projection of the Euclidean gradient onto the tangent space ([13, Equation 3.37]). With these, the above equality can be further simplified to,

$$\langle \nabla_x f, \text{Retr}_x(\eta) - x \rangle = \langle \text{grad}_{x_1} f, \eta_1 \rangle + \langle \text{grad}_{x_2} f, \eta_2 \rangle + \langle \nabla_{x_1} f, \text{Retr}_{x_1}(\eta_1) - x_1 - \eta_1 \rangle \quad (92)$$

$$= \langle \text{grad}_x f, \eta \rangle + \langle \nabla_{x_1} f, \text{Retr}_{x_1}(\eta_1) - x_1 - \eta_1 \rangle. \quad (93)$$

Plugging (93) into (87) gives,

$$\begin{aligned} |f(y) - [f(x) + \langle \nabla_x f, y - x \rangle]| &= |f(\text{Retr}_x(\eta)) - [f(x) + \langle \text{grad}_x f, \eta \rangle + \langle \nabla_{x_1} f, \text{Retr}_{x_1}(\eta_1) - x_1 - \eta_1 \rangle]| \\ &\leq \frac{L}{2} \|\text{Retr}_x(\eta) - x\|^2. \end{aligned} \quad (94)$$

Applying the triangle and Cauchy-Schwarz inequalities and expanding $\|\text{Retr}_x(\eta) - x\|^2$ yields,

$$|f(\text{Retr}_x(\eta)) - [f(x) + \langle \text{grad}_x f, \eta \rangle]| \leq \frac{L}{2} \|\text{Retr}_x(\eta) - x\|^2 + \langle \nabla_{x_1} f, \text{Retr}_{x_1}(\eta_1) - x_1 - \eta_1 \rangle \quad (95)$$

$$\leq \frac{L}{2} \|\text{Retr}_x(\eta) - x\|^2 + \|\nabla_{x_1} f\| \|\text{Retr}_{x_1}(\eta_1) - x_1 - \eta_1\| \quad (96)$$

$$= \frac{L}{2} \|\eta_2\|^2 + \frac{L}{2} \|\text{Retr}_{x_1}(\eta_1) - x_1\|^2 + \|\nabla_{x_1} f\| \|\text{Retr}_{x_1}(\eta_1) - x_1 - \eta_1\|. \quad (97)$$

As $\nabla_{x_1} f$ is continuous on the compact set \mathcal{M}_1 , there exists finite G_1 such that $\|\nabla_{x_1} f\| \leq G_1$ for all $x_1 \in \mathcal{M}_1$. In equations (B.3) and (B.4) in [44], Boumal et al. show that for the compact submanifold \mathcal{M}_1 , the following inequalities hold,

$$\|\text{Retr}_{x_1}(\eta_1) - x_1\| \leq \alpha_1 \|\eta_1\|, \quad (98)$$

$$\|\text{Retr}_{x_1}(\eta_1) - x_1 - \eta_1\| \leq \beta_1 \|\eta_1\|^2, \quad (99)$$

for some $\alpha_1, \beta_1 \geq 0$. Plugging (98) and (99) in (97) gives,

$$|f(\text{Retr}_x(\eta)) - [f(x) + \langle \text{grad}_x f, \eta \rangle]| \leq \frac{L}{2} \|\eta_2\|^2 + \frac{L}{2} \alpha_1^2 \|\eta_1\|^2 + G_1 \beta_1 \|\eta_1\|^2. \quad (100)$$

Let $c_g \triangleq \max\left(\frac{L}{2}, \frac{L\alpha_1^2}{2} + G_1\beta_1\right)$. From (100) it trivially holds that,

$$|f(\text{Retr}_x(\eta)) - [f(x) + \langle \text{grad}_x f, \eta \rangle]| \leq c_g (\|\eta_1\|^2 + \|\eta_2\|^2) = c_g \|\eta\|^2. \quad (101)$$

□

Proof of Lemma 1. We separately show that each cost function has Lipschitz-type gradient for pullbacks.

1. Single rotation update (Section 4.3). Recall that this case, our cost function (24) is defined on the Stiefel manifold $\text{St}(d, r)$. It is straightforward to verify that same cost function defined on the ambient space $\mathbb{R}^{r \times d}$ has Lipschitz continuous gradient, with the Lipschitz constant given by $\kappa_i \triangleq \sum_{j \in N_{\text{out}}(i)} \kappa_{ij} + \sum_{k \in N_{\text{in}}(i)} \kappa_{ki}$. Since Stiefel manifold is compact, invoking Lemma 4 shows that $f : \text{St}(d, r) \rightarrow \mathbb{R}$ has Lipschitz-type gradient for pullbacks.
2. Single pose update (Section 4.4). Our cost function (27) is defined on the product manifold $\text{St}(d, r) \times \mathbb{R}^r$. Similar to the previous case, it is straightforward to verify that the same cost function defined on the ambient space $\mathbb{R}^{r \times d} \times \mathbb{R}^r$ has Lipschitz continuous gradient. Invoking Lemma 5 with $\mathcal{M}_1 = \text{St}(d, r)$ and $\mathcal{E}_2 = \mathbb{R}^r$ shows that $f : \text{St}(d, r) \times \mathbb{R}^r \rightarrow \mathbb{R}$ has Lipschitz-type gradient for pullbacks.
3. Multiple rotations update (Section 4.2). The cost function (20) is defined on the product manifold $\text{St}(d, r)^{n_\alpha}$. The same cost defined on the ambient space $\mathbb{R}^{r \times dn_\alpha}$ has Lipschitz continuous gradient with the Lipschitz constant given by the maximum eigenvalue of $Q_{\mathbb{R}[\alpha, \alpha]}$. Since the Cartesian product of compact sets is compact, invoking Lemma 4 shows that $f : \text{St}(d, r)^{n_\alpha} \rightarrow \mathbb{R}$ has Lipschitz-type gradient for pullbacks.
4. Multiple poses update (Section 4.2). In this case, we can view the cost function (21) as defined on the product manifold $\text{St}(d, r)^{n_\alpha} \times \mathbb{R}^{r \times n_\alpha}$, where we have separated the rotation and translation components. Similar to the previous case, the same cost function defined on the ambient space $\mathbb{R}^{r \times dn_\alpha} \times \mathbb{R}^{r \times n_\alpha}$ has Lipschitz continuous gradient with the Lipschitz constant given by the maximum eigenvalue of $Q_{\mathbb{T}[\alpha, \alpha]}$. Invoking Lemma 5 with $\mathcal{M}_1 = \text{St}(d, r)^{n_\alpha}$ and $\mathcal{E}_2 = \mathbb{R}^{r \times n_\alpha}$ shows that $f : \text{St}(d, r)^{n_\alpha} \times \mathbb{R}^{r \times n_\alpha} \rightarrow \mathbb{R}$ has Lipschitz-type gradient for pullbacks.

□

E Proof of Lemma 2

Proof of Lemma 2. Our proof largely follows the proof of Lemma 3.11 in [44]. Recall that at each iteration of Algorithm 2, we use RTR to optimize block b by solving,

$$\underset{x_b \in \mathcal{M}_b}{\text{minimize}} \quad f_b(x_b). \quad (102)$$

By Assumption 1, f_b satisfies (34) globally with Lipschitz constant $c_b \geq 0$. With a slight abuse of notation, we use $x_b = x_{b_t}^t$ to denote the initial value of the selected block. Define $g_b \triangleq \text{grad}_{x_{b_t}^t} f_b = \text{grad}_{x_{b_t}^t} f$. For notation convenience, in the remaining proof we use η to represent a tangent vector in $T_{x_b} \mathcal{M}_b$. Using the simplified notation, we can write the first trust-region subproblem as,

$$\underset{\eta \in T_{x_b} \mathcal{M}_b}{\text{minimize}} \quad \hat{m}_{x_b}(\eta) = f_b(x_b) + \langle \eta, g_b \rangle + \frac{1}{2} \langle \eta, H[\eta] \rangle, \quad (103a)$$

$$\text{subject to} \quad \|\eta\| \leq \Delta_0. \quad (103b)$$

Recall that Δ_0 above is the initial trust-region radius. By Assumption 2, there exists $c_0 \geq 0$ such that $\langle \eta, H[\eta] \rangle \leq c_0 \|\eta\|^2$ for all $\eta \in T_{x_b} \mathcal{M}_b$. Define the constant,

$$\lambda_b \triangleq \frac{1}{4} \min \left(\frac{1}{c_0}, \frac{1}{2c_b + 2c_0} \right) = \frac{1}{8(c_b + c_0)}. \quad (104)$$

Note that λ_b is the same constant defined in Assumption 2. Following [44], in the next part of this proof, we make the additional assumption that the initial trust-region radius Δ_0 is also bounded above by $\Delta_0 \leq 4\lambda_b \|g_b\|$. We show how we can remove this assumption safely at the end of this proof.

We show that the required cost decrement in Lemma 2 is achieved by taking the so-called *Cauchy step* [44] in the first trust-region subproblem. By definition, the Cauchy step η^C minimizes (103) along the direction of the negative Riemannian gradient, i.e., $\eta^C = -\alpha^C g_b$. The step size $\alpha^C \in [0, \Delta_0/\|g_b\|]$ can be determined in closed-form as,

$$\alpha^C = \begin{cases} \min\left(\frac{\|g_b\|^2}{\langle g_b, H[g_b] \rangle}, \frac{\Delta_0}{\|g_b\|}\right), & \text{if } \langle g_b, H[g_b] \rangle > 0, \\ \frac{\Delta_0}{\|g_b\|}, & \text{otherwise.} \end{cases} \quad (105)$$

A straightforward calculation (see [44, Lemma 3.7]) shows that the Cauchy step reduces the model function \hat{m}_{x_b} by at least,

$$\hat{m}_{x_b}(0) - \hat{m}_{x_b}(\eta^C) \geq \frac{1}{2} \min\left(\Delta_0, \frac{\|g_b\|}{c_0}\right) \|g_b\|. \quad (106)$$

Next, we need to relate the above model decrement (106) with the actual decrement of the cost function f_b . For this, we show that the following ratio,

$$\left| \frac{\hat{f}_{x_b}(0) - \hat{f}_{x_b}(\eta^C)}{\hat{m}_{x_b}(0) - \hat{m}_{x_b}(\eta^C)} - 1 \right| = \left| \frac{\hat{m}_{x_b}(\eta^C) - \hat{f}_{x_b}(\eta^C)}{\hat{m}_{x_b}(0) - \hat{m}_{x_b}(\eta^C)} \right| \quad (107)$$

is close to zero. Note that in (107) we use the fact that, by definition, $\hat{m}_{x_b}(0) = \hat{f}_{x_b}(0) = f_b(x_b)$. We derive an upper bound on the numerator of (107) as follows,

$$|\hat{m}_{x_b}(\eta^C) - \hat{f}_{x_b}(\eta^C)| = |f_b(x_b) + \langle g_b, \eta^C \rangle + \frac{1}{2} \langle \eta^C, H[\eta^C] \rangle - \hat{f}_{x_b}(\eta^C)| \quad (\text{Definition of } \hat{m}_{x_b}) \quad (108)$$

$$\leq |f_b(x_b) + \langle g_b, \eta^C \rangle - \hat{f}_{x_b}(\eta^C)| + \frac{1}{2} |\langle \eta^C, H[\eta^C] \rangle| \quad (\text{Triangle inequality}) \quad (109)$$

$$\leq \frac{1}{2} (c_b + c_0) \|\eta^C\|^2. \quad (110)$$

For the last inequality, we have used the Lipschitz-type gradient condition of f_b for the first term, and the boundedness of H for the second term. Plugging (106) and (110) into (107), we obtain,

$$\left| \frac{\hat{f}_{x_b}(0) - \hat{f}_{x_b}(\eta^C)}{\hat{m}_{x_b}(0) - \hat{m}_{x_b}(\eta^C)} - 1 \right| \leq \frac{\frac{1}{2} (c_b + c_0) \|\eta^C\|^2}{\frac{1}{2} \min(\Delta_0, \frac{\|g_b\|}{c_0}) \|g_b\|} \quad (\text{106 and 110}) \quad (111)$$

$$\leq \frac{(c_b + c_0) \Delta_0^2}{\min(\Delta_0, \frac{\|g_b\|}{c_0}) \|g_b\|} \quad (\|\eta^C\| \leq \Delta_0) \quad (112)$$

$$\leq \frac{(c_b + c_0) \Delta_0}{\|g_b\|}. \quad (\min(\Delta_0, \|g_b\|/c_0) \leq \Delta_0) \quad (113)$$

Next, using our additional assumption that $\Delta_0 \leq 4\lambda_b \|g_b\| \leq \|g_b\|/(2c_b + 2c_0)$, (113) implies,

$$\left| \frac{\hat{f}_{x_b}(0) - \hat{f}_{x_b}(\eta^C)}{\hat{m}_{x_b}(0) - \hat{m}_{x_b}(\eta^C)} - 1 \right| \leq \frac{1}{2} \implies \rho \triangleq \frac{\hat{f}_{x_b}(0) - \hat{f}_{x_b}(\eta^C)}{\hat{m}_{x_b}(0) - \hat{m}_{x_b}(\eta^C)} \geq \frac{1}{2}. \quad (114)$$

In particular, ρ is bigger than the acceptance threshold of RTR (see (38)) and thus η^C is *guaranteed* to be accepted. Furthermore, we also have,

$$\hat{f}_{x_b}(0) - \hat{f}_{x_b}(\eta^C) \geq \frac{1}{2} (\hat{m}_{x_b}(0) - \hat{m}_{x_b}(\eta^C)) \quad (114) \quad (115)$$

$$\geq \frac{1}{4} \min\left(\Delta_0, \frac{\|g_b\|}{c_0}\right) \|g_b\| \quad (106) \quad (116)$$

$$\geq \frac{1}{4} \min\left(\lambda_b, \frac{1}{c_0}\right) \|g_b\|^2 \quad (\Delta_0 \geq \lambda_b \|g_b\| \text{ by Assumption 2}) \quad (117)$$

$$= \frac{1}{4} \lambda_b \|g_b\|^2. \quad (\lambda_b \leq 1/c_0 \text{ by definition}) \quad (118)$$

Note that $\hat{f}_{x_b}(0) - \hat{f}_{x_b}(\eta^C)$ is exactly the global cost decrement if block x_b is updated with the Cauchy step. Thus, we have shown that under the additional assumption that $\Delta_0 \leq 4\lambda_b\|g_b\|$, the desired cost decrement is guaranteed by taking the Cauchy step in the first trust-region subproblem. Since RTR is a descent algorithm, additional iterations will only reduce the cost further.

To complete the proof, note that if we drop the additional assumption and $\Delta_0 > 4\lambda_b\|g_b\|$, (114) might fail to hold and as a result the Cauchy step can be rejected in the first trust-region subproblem. However, by the mechanism of RTR, after each rejection the trust-region radius will be divided by four in the next iteration (see (39)). Therefore, in the worst case, the trust-region radius will be within the interval $[\lambda_b\|g_b\|, 4\lambda_b\|g_b\|]$ after $O(\log(4\lambda_b\|g_b\|\Delta_0))$ consecutive rejections, after which the Cauchy step is guaranteed to be accepted in the next trust-region subproblem. \square

F Proof of Theorem 3

Proof of Theorem 3. We prove the convergence of Algorithm 2 with all three block selection rules.

Uniform Sampling. We first prove the convergence of Algorithm 2 with uniform sampling. By Lemma 2, at iteration t the global cost is decreased by at least,

$$f(x^t) - f(x^{t+1}) \geq \frac{1}{4}\lambda_{b_t}\|\text{grad}_{x_{b_t}} f\|^2, \quad (119)$$

where $b_t \in [n_b]$ is the updated block at this iteration, selected uniformly at random. Taking the expectation with respect to b_t conditioned on $b_{0:t-1}$ yields,

$$f(x^t) - \mathbb{E}_{b_t|b_{0:t-1}}f(x^{t+1}) = \mathbb{E}_{b_t|b_{0:t-1}}[f(x^t) - f(x^{t+1})] \quad (\mathbb{E}_{b_t|b_{0:t-1}}f(x^t) = f(x^t)) \quad (120)$$

$$\geq \sum_{b \in [n_b]} \frac{1}{n_b} \cdot \frac{1}{4}\lambda_b\|\text{grad}_{x_b} f\|^2 \quad (\text{Lemma 2 and uniform sampling}) \quad (121)$$

$$\geq \frac{\min_{b \in [n_b]} \lambda_b}{4n_b} \|\text{grad}_{x^t} f\|^2. \quad (122)$$

Next, apply the law of total expectation gives,

$$f(x^0) - f^* \geq f(x^0) - \mathbb{E}_{b_{0:T-1}}f(x^T) \quad (f^* \text{ is the global minimum}) \quad (123)$$

$$= \sum_{t=0}^{T-1} \mathbb{E}_{b_{0:t}}[f(x^t) - f(x^{t+1})] \quad (\mathbb{E}_{b_{0:t}}f(x^t) = \mathbb{E}_{b_{0:t-1}}f(x^t)) \quad (124)$$

$$= \sum_{t=0}^{T-1} \mathbb{E}_{b_{0:t-1}}[f(x^t) - \mathbb{E}_{b_t|b_{0:t-1}}f(x^{t+1})] \quad (\text{Law of Total Expectation}) \quad (125)$$

$$\geq \sum_{t=0}^{T-1} \mathbb{E}_{b_{0:t-1}}\left[\frac{\min_{b \in [n_b]} \lambda_b}{4n_b} \|\text{grad}_{x^t} f\|^2\right] \quad (122) \quad (126)$$

$$\geq T \cdot \frac{\min_{b \in [n_b]} \lambda_b}{4n_b} \min_{0 \leq t \leq T-1} \mathbb{E}_{b_{0:t-1}} \|\text{grad}_{x^t} f\|^2. \quad (127)$$

Rearranging the last inequality gives (45).

Importance Sampling. Recall that with importance sampling, at iteration t block b is selected with probability $p_b = \|\text{grad}_{x_b} f\|^2 / \|\text{grad}_{x^t} f\|^2$. Once again, taking the expectation with respect to b_t conditioned on $b_{0:t-1}$

gives,

$$f(x^t) - \mathbb{E}_{b_t|b_{0:t-1}} f(x^{t+1}) \geq \sum_{b \in [n_b]} \frac{\|\text{grad}_{x_b^t} f\|^2}{\|\text{grad}_{x^t} f\|^2} \cdot \frac{1}{4} \lambda_b \|\text{grad}_{x_b^t} f\|^2 \quad (128)$$

$$\geq \frac{\min_{b \in [n_b]} \lambda_b}{4} \cdot \frac{\sum_{b \in [n_b]} \|\text{grad}_{x_b^t} f\|^4}{\sum_{b \in [n_b]} \|\text{grad}_{x_b^t} f\|^2} \quad (129)$$

$$= \frac{\min_{b \in [n_b]} \lambda_b}{4} \cdot \frac{\sum_{b \in [n_b]} a_b^2}{\sum_{b \in [n_b]} a_b}, \quad (130)$$

where we define $a_b \triangleq \|\text{grad}_{x_b^t} f\|^2$ for brevity. Applying the Cauchy-Schwarz inequality gives,

$$\frac{1}{n_b^2} \left(\sum_{b \in [n_b]} a_b \right)^2 \leq \frac{1}{n_b} \sum_{b \in [n_b]} a_b^2. \quad (131)$$

Rearranging the above inequality yields,

$$\frac{\sum_{b \in [n_b]} a_b^2}{\sum_{b \in [n_b]} a_b} \geq \frac{1}{n_b} \sum_{b \in [n_b]} a_b = \frac{1}{n_b} \|\text{grad}_{x^t} f\|^2. \quad (132)$$

Combining (130) and (132) gives,

$$f(x^t) - \mathbb{E}_{b_t|b_{0:t-1}} f(x^{t+1}) \geq \frac{\min_{b \in [n_b]} \lambda_b}{4n_b} \|\text{grad}_{x^t} f\|^2. \quad (133)$$

The rest of the proof is identical to the proof for uniform sampling.

Greedy Selection. By the greedy selection mechanism, at iteration t the global cost is decreased by at least,

$$f(x^t) - f(x^{t+1}) \geq \frac{1}{4} \lambda_{b_t} \|\text{grad}_{x^t} f\|_{\mathcal{B}}^2 \quad (\text{Lemma 2 and Definition 3}) \quad (134)$$

$$\geq \frac{1}{4} \min_{b \in [n_b]} \lambda_b \cdot \|\text{grad}_{x^t} f\|_{\mathcal{B}}^2. \quad (\lambda_{b_t} \geq \min_{b \in [n_b]} \lambda_b) \quad (135)$$

Above, $\|\cdot\|_{\mathcal{B}}$ is the maximum block norm defined in Definition 3. A telescoping sum of the above inequalities from $t = 0$ to $t = T - 1$ gives,

$$f(x^0) - f^* \geq \sum_{t=0}^{T-1} \frac{1}{4} \min_{b \in [n_b]} \lambda_b \cdot \|\text{grad}_{x^t} f\|_{\mathcal{B}}^2 \quad (136)$$

$$\geq \frac{T}{4} \cdot \min_{b \in [n_b]} \lambda_b \cdot \min_{0 \leq t \leq T-1} \|\text{grad}_{x^t} f\|_{\mathcal{B}}^2. \quad (137)$$

Rearranging the last inequality gives (46). □